2(mix)

N71-21514

THERMAL ACTIVE OPTICS TECHNIQUE FOR CORRECTING SYMMETRICAL DISTORTIONS IN SPACE TELESCOPE MIRRORS

A Thesis

Presented to

the Faculty of the School of Engineering and Applied Science

University of Virginia

In Partial Fulfillment

of the Requirements for the Degree

Master of Science in Mechanical Engineering

by

Marvin D. Rhodes

September 1970

APPROVAL SHEET

This thesis is submitted in partial fulfillment of
the requirements for the degree of
Master of Science in Mechanical Engineering

Author

Approved:

Thesis Advisor

Faculty Advisor

Dean, School of Engineering and
Applied Science

September 1970

ABSTRACT

Orbiting astronomical observations have the potential for making observations far superior to those from earth-based mirrors. In order for this performance to be realized, the contour of the primary mirror must be very accurately controlled. A thermally activated system for correcting symmetrical distortions in space telescope mirrors has been evaluated. This system utilizes thermally induced elastic strains to correct axial distortions in the mirror. The relation between axial distortion and thermal inputs was determined by a finite difference solution of the equations for thin elastic shells.

The use of this technique was demonstrated analytically on a beryllium paraboloid. This mirror had 10 equally spaced thermal inputs. Distortions due to an acceleration-type loading were shown to be corrected to well within the required accuracy. Axial temperature gradients resulting from the application of the thermal inputs to the rear surface of the mirror were shown to be quite small.

ACKNOWLEDGMENTS

The author would like to express his gratitude to the National Aeronautics and Space Administration for their support, and to Dr. E. T. Kruszewski of Langley Research Center and Dr. J. Taylor Beard of the University of Virginia for their guidance during this investigation.

TABLE OF CONTENTS

LIST OF TABLES

$\epsilon_\xi, \epsilon_\theta$	elastic strains (see eq. (61))
λ	separation constant (see eqs. (31) and (32))
ν	Poisson's ratio
ξ, θ, ζ	rectangular coordinate system, ξ is along the meridian of the shell, θ is measured along the circumference, and ζ is normal to the shell surface
ξ_n	meridional distance to the location of control point n
ρ	radial coordinate
ρ_n	radial distance to the location of control point n
ρ_t	radius of disc over which thermal input is applied (see Fig. 8)
$\sigma_\xi, \sigma_\theta$	normal stresses in the shell
σ	Stefan-Boltzmann constant, 1.713×10^{-9} Btu/hr-ft^2-$^\circ$R^4
$\lvert \phi \rvert$	column matrix of thermal inputs
φ	angular coordinate, angle between mirror axis and radius of curvature (see Fig. 12)
χ_ξ	rotation of the neutral surface of the paraboloidal shell (see Fig. 14)
ψ	angle between normal to circular disc and line connecting mirror and telescope port (see Fig. 9)

CHAPTER I

INTRODUCTION

The resolution of ground-based optical astronomical observatories is limited by atmospheric turbulence. To minimize the effects of turbulence, many observatories are located at relatively inaccessible areas atop tall mountains. Even at these locations the very best telescopes seldom have a resolution better than 0.3 second of arc. In space, telescopes would be limited only by the diffraction limit and, therefore, large mirrors (120 in. dia.) should be able to resolve 0.03 arc second at 5,000 angstroms (Ref. 1). Also, space telescopes will be able to view portions of the spectrum not currently available for observation due to atmospheric absorption.

The National Aeronautics and Space Administration is currently investigating the problems associated with the operation of large (120 in. dia. aperture) space telescopes. Several studies of space telescopes have been conducted and are reported in References 2, 3, and 4. These studies have defined the scientific objectives of a space telescope and outlined some of the major problems involved in its design and fabrication. All of these studies have recommended the use of a Cassegrain optical system which requires a paraboloidal primary mirror. In order for the optical system to have the desired resolution, the contour of the primary mirror must be maintained to within 2 microinches of the design value (Ref. 3). If this accuracy cannot be maintained, the resolution of space telescopes will be

degraded relative to their potential capabilities and their performance may be less than that of ground-based observatories.

Two types of primary mirrors have been proposed for use in space telescopes. The first type is a passive mirror which would be designed to retain the proper contour without correction for the life of the telescope. This mirror would consequently be rather massive and may impose a severe weight penalty on the launch booster. The second concept is known as an active optics system and utilizes a thin mirror which is permitted to deform moderately under operational loads. Distortions in the mirror would be monitored and analyzed by a figure error sensor. This sensor would activate a control system to apply correction loads which would remove the distortions.

One active optics system utilizing precision jacks to provide corrective loads has been investigated analytically. This analysis has been experimentally verified using a thin deformable mirror 30 inches in diameter (Ref. 5). However, this system requires either a very stiff back plate for the jacks to react against or a determination of the coupling between the back plate and the mirror. Also, this is an electromechanical system and is relatively complicated for space use. Another type of active optics system that has been suggested utilizes thermal inputs to provide the corrective distortions. Elastic strains introduced by differential heating would be used to force the mirror to assume the proper contour.

The object of this investigation is to develop a technique for determining the relation between deformations parallel to the mirror

axis and the thermal inputs necessary for error correction in such a system. Thermal inputs in the form of a prescribed temperature distribution were considered to be applied to the rear surface of the mirror. In order to illustrate the feasibility of such a technique, a cosine-type temperature profile was considered for the loading. The axial temperature gradient introduced in the mirror due to front surface radiation loss was shown to be small. The relation between the mirror distortions and the thermal inputs was obtained by a computerized finite difference solution of the elastic shell equations. The relation was expressed in the form of a flexibility matrix. The thermal inputs necessary to correct distortion at specific control points were determined by inverting the flexibility matrix to form a stiffness matrix. An example of the thermal inputs necessary to correct distortions due to an acceleration-type loading is shown.

CHAPTER II

THERMAL CONTROL SYSTEM

Description of Telescope

The space-telescope model selected for this analysis is a preliminary design of the type discussed in Reference 3. A sketch of this model is shown in Figure 1. The basic telescope configuration consists of two large cylindrical shells which are attached to the telescope cabin. The cylindrical shells enclose the main optical elements - the primary and secondary mirrors. Attached to the outer shell is a system of doors that prevents sunlight from falling on the optical system during maneuvers. The inner shell is a thermal shield which reduces solar heating loads on the primary mirror. All optical imaging devices and sensing instruments are contained in the telescope cabin. This cabin will also provide the necessary environment for manned support. One significant departure from previously designed space systems is that the telescope must be capable of continuous operation for several years. Therefore, the telescope must receive manned support from a docked or nearby space station.

The telescope has a Cassegrain-type optical system with a focal-length-to-aperture diameter (f/d) of 30. The primary mirror is a short-focal-length (f/d = 4) paraboloid, while the smaller secondary mirror is a hyperboloid. If this optical system could be fabricated with perfect geometry it would image a point source, such as a star, in the focal plane as a bright central disc (Airy disc) with

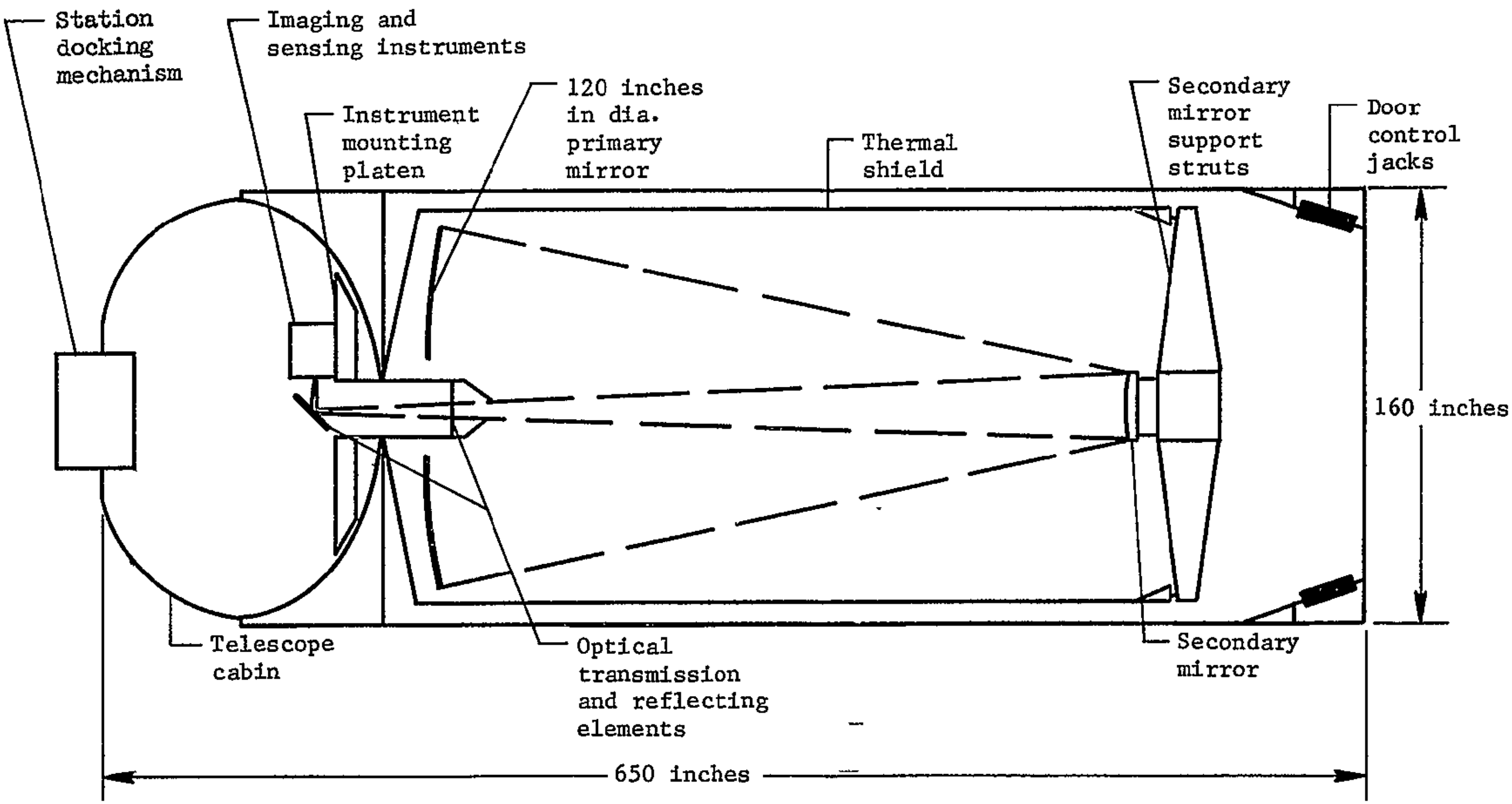

Figure 1.- Sketch of an orbiting space telescope.

surrounding diffraction rings. The Airy disc would contain approximately 85 per cent of the incident energy with the remaining 15 per cent scattered in the surrounding rings. However, due to fabrication errors in the mirrors, operating loads and inherent absorption losses, the energy in the central disc will be reduced and the resolving power of the telescope may be severely limited. If the distortions in the optical system are such that 68 per cent of the energy lies in the central disc with 32 per cent in the diffraction rings, the system is operating at the Rayleigh criterion for resolution. An analysis of the optical system for this diffraction-limited operation was considered in Reference 3. This analysis estimates that the primary mirror will require a surface contour having distortions less than 1.97 microinches (1/10 wavelength at 5,000 angstroms) from the design paraboloid. In addition, a root-mean-square surface accuracy of 0.37 microinch (1/53 wavelength at 5,000 angstroms) will be required.

It was noted previously that distortions in the optical system may be produced by operational loads. Other sources of distortion may include (1) the introduction of elastic strains in changing from an earth gravity environment to a zero gravity space environment, (2) relaxation of residual strains introduced during the fabrication of the mirror billet, (3) relaxation of residual strains introduced by machining and polishing operations, and (4) plastic strains introduced by launch and environmental loads.

Thermal Active Optics System

In order to maintain the mirror contour within the required accuracy, a technique to introduce corrective distortions may be necessary. The technique envisioned in this analysis for correcting mirror distortions is to apply thermal inputs to the rear surface of the mirror. These thermal loads will induce elastic strains which will deform the mirror surface to the desired paraboloidal contour. A schematic diagram of a thermal active optics system is shown in Figure 2. Distortions in the primary mirror are detected by the figure error sensor using interferometric techniques. These errors are in the form of fringe patterns and must be interpreted to determine the size and direction of the distortion. This interpretation is performed by the analyzer and phase detector at fixed control points on the mirror surface. The analyzer will also calculate the amplitude of the controlled temperature source necessary to correct distortions at the control points. The function of the control system is to apply the desired inputs, thereby reducing the distortions at the control points to (or below) the acceptable level.

A sketch illustrating the control points and location of the thermal inputs is shown in Figure 3. The thermal inputs are in the form of controlled back surface temperature distributions. The radial and circumferential location of the thermal inputs, in addition to their size, may vary. It is only necessary to determine the influence of the thermal inputs at specific control points on the surface.

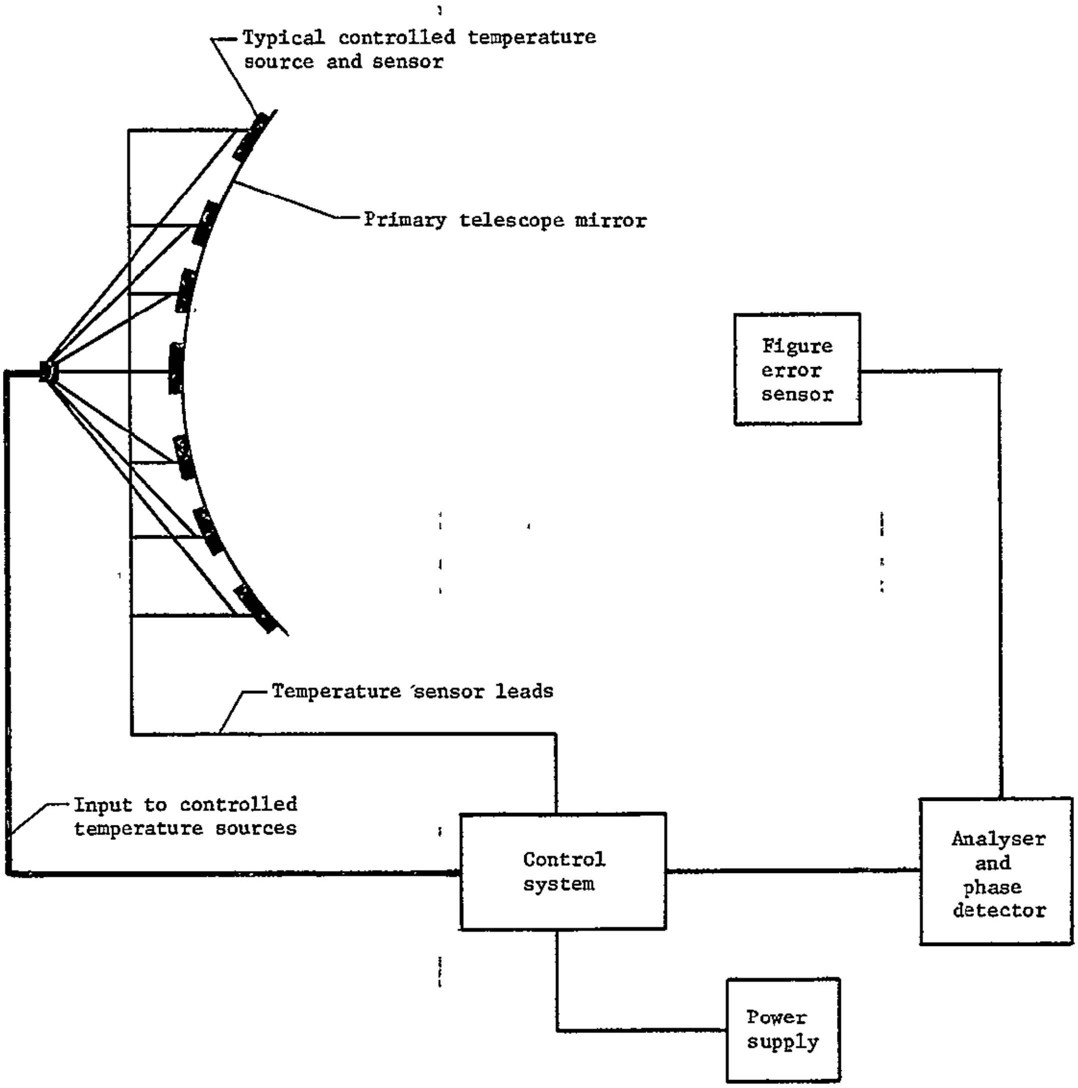

Figure 2.- Schematic of thermal active optics system.

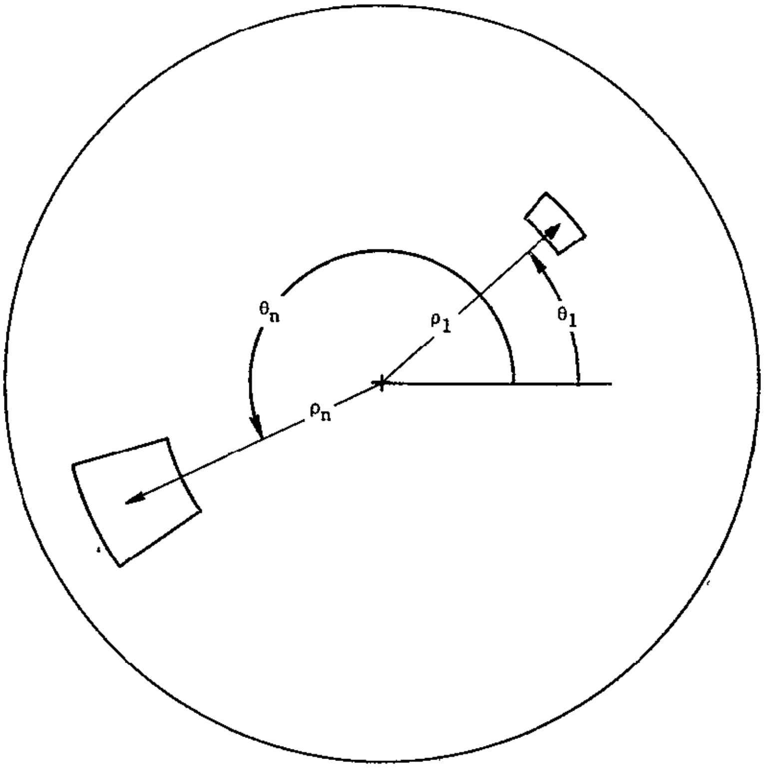

Figure 3.- Sketch showing control points and location of thermal inputs on rear surface of telescope mirror.

Most practical structures, including the telescope mirror discussed in Reference 5 have been shown to exhibit approximate linear behavior. In order to determine the influence of the thermal inputs, it was assumed in this analysis that the thin paraboloidal shell behaves as a linear structure. Thus the influence of thermal inputs can be analyzed using linear theory. One advantage of such a structural theory is that it permits the application of the principle of superposition. This principle states that stresses and deformations produced in a structure by a set of loads in combination can be obtained by adding the stresses and deformations produced by each load acting

separately. Therefore, the distortions at the control points may be expressed as a function of the applied thermal inputs by the following equations:

$$\left.\begin{aligned}
\delta_1 &= c_{11}T_1 + c_{12}T_2 + c_{13}T_3 + c_{14}T_4 + \cdots c_{1n}T_n \\
\delta_2 &= c_{21}T_1 + c_{22}T_2 + c_{23}T_3 + c_{24}T_4 + \cdots c_{2n}T_n \\
&\vdots \\
\delta_n &= c_{n1}T_1 + c_{n2}T_2 + c_{n3}T_3 + c_{n4}T_4 + \cdots c_{nn}T_n
\end{aligned}\right\} \tag{1}$$

The coefficients (c_{ij}) specify the contribution due to an increase in temperature from each thermal input (T_j) toward the distortion (δ_i) at the control point (i). These equations may be written in the more convenient matrix notation as

$$|\delta| = \left[C\right] |T| \tag{2}$$

The square matrix $\left[C\right]$ is generally called the structure flexibility matrix and the component terms are deflection influence coefficients.

The thermal inputs necessary to correct mirror distortions can be expressed by inverting the flexibility matrix and multiplying by the measured distortions.

$$|T| = \left[K\right] |\delta| \tag{3}$$

where

$$\left[K\right] = \left[C\right]^{-1}$$

In order for the active optics system to perform properly it is necessary to accurately determine the coefficients k_{ij} for each control point and store the coefficients in the system analyzer.

CHAPTER III

THERMAL ANALYSIS

Description of Mirror Geometry

No firm design of the space telescope has been formulated. The technique developed in this investigation is applicable to any thin telescope mirror. The example shown in this and subsequent sections illustrates the use of this technique.

A sketch of the mirror used in this analysis is shown in Figure 4. The mirror is a thin paraboloidal shell having a diameter of 120 inches and a focal length of 480 inches. Since no firm design of the telescope has been formulated, certain assumptions concerning the mirror geometry were necessary. For example, the diameter of the

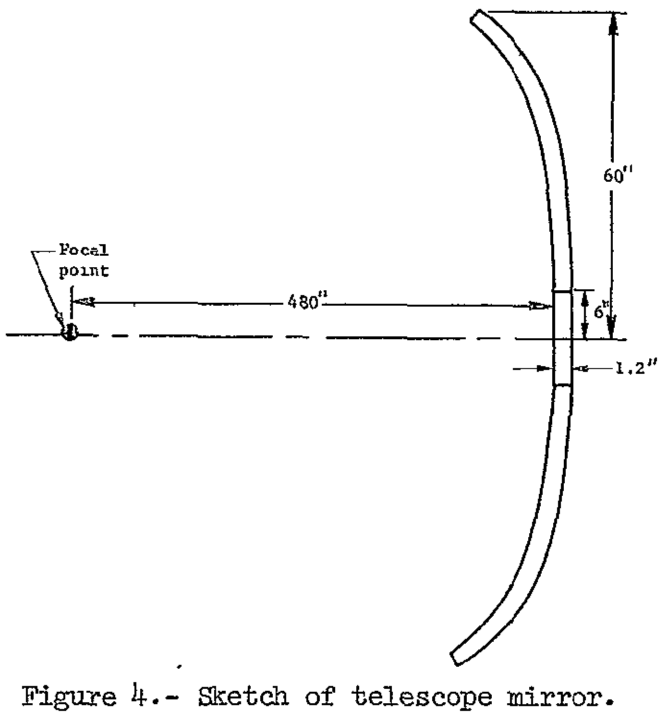

Figure 4.- Sketch of telescope mirror.

center hole will depend upon the telescope optical system and manufacturing considerations. The hole was assumed to have a diameter equal to one-tenth (12 inches) the diameter of the mirror. In the weightless environment of space, only a very thin reflective surface would be necessary for the primary mirror. However, practical considerations of manufacture will require the mirror to be sufficiently thick to withstand grinding and polishing in a gravity environment. For this investigation, the thickness of the mirror was one-hundredth (1.2 inches) of the diameter (Ref. 7). The thickness was assumed to be constant in both the circumferential and meridional directions.

Metal mirrors are ideally suited for thin one-piece construction because they have high stiffness-to-weight ratios. Beryllium has one of the highest stiffness-to-weight ratios of any structural metal and is currently being considered as one of the prime candidate materials for telescope mirrors (Ref. 8). The paraboloid shown in Figure 4 was considered to be fabricated from a homogeneous and isotropic billet of beryllium. The properties of the beryllium material for this mirror are shown in Table I.

The mirror was restrained at the outer rim by a system which accommodates only symmetrical loading about the mirror axis. This support system restrains the mirror only in the axial direction and is usually referred to as a hinged support on rollers. A sketch of the support condition is shown in Figure 5. This system is similar to a three-point tangent-bar mounting suspension considered in Reference 3. The systems are similar in that both will accommodate differential

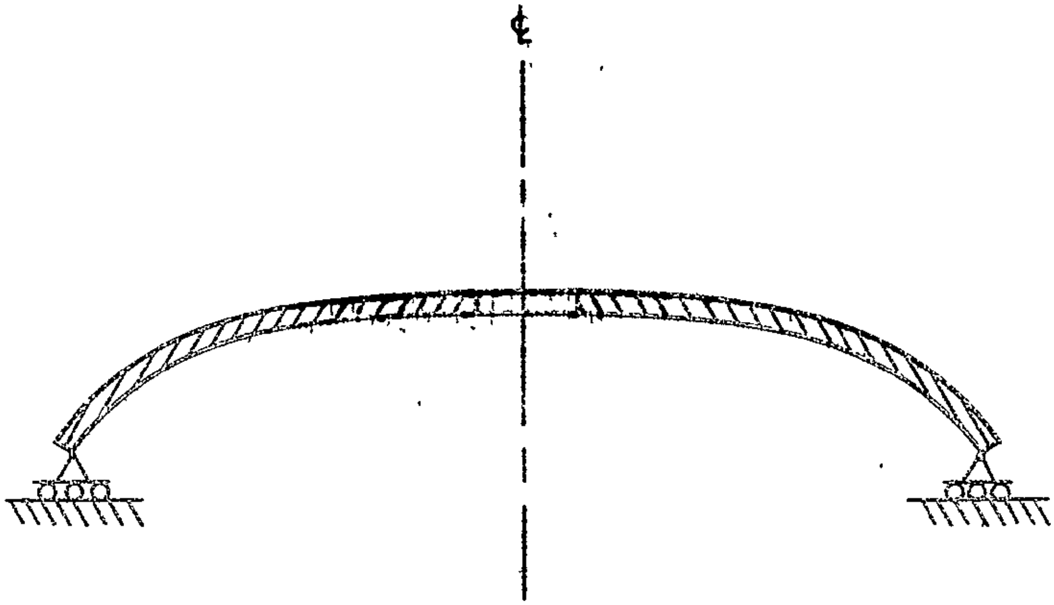

Figure 5.- Sketch of mirror cross section illustrating boundary conditions.

radial expansion between the mirror and support structure without introducing loads in the mirror. No restraints were applied at the central cutout portion of the mirror.

For the illustration of the thermal active optics system, symmetrical distortions of the primary mirror were considered. Sources with a controlled temperature distribution were selected to provide the thermal inputs. The controlled sources were applied to the rear surface of the mirror. In order to simplify the problem, only steady-state distortions were examined. Therefore, the results of this study are applicable only if observations are made after steady-state conditions exist.

Ten equally spaced stations along the meridian of the mirror were selected as the control points. The location of these stations is shown in Figure 6. The points were separated by a meridional distance of 5.404 inches. Ten control points were considered to be a sufficient number to demonstrate this technique. The use of more control points would only have generated a larger matrix of influence coefficients and would have added little to the demonstration of the technique. For an actual control system, a larger number of heaters may be desirable to increase the control capability. No control point was located at the periphery of the shell because of the axial restraint imposed by the boundary condition. A thermal input at that location, however, would influence the distortion at the other control points.

The thermal inputs applied by the strip heaters to the rear surface of the mirror were assumed to have the form

$$T_n \begin{cases} = A\left(\frac{1}{2} + \frac{1}{2}\cos\frac{\pi(\xi - \xi_n)}{\frac{\Delta}{4}}\right) & |\xi - \xi_n| \leq \frac{\Delta}{4} \\ = 0 & |\xi - \xi_n| > \frac{\Delta}{4} \end{cases} \tag{5}$$

A sketch of this thermal input applied at a control point on the mirror surface is shown in Figure 7. Thermal inputs of this form were selected because they can be represented by a concise mathematical expression. Also, these inputs should be relatively easy to simulate experimentally since they produce no severe radial gradients. It should be noted in the figure that the thermal inputs were applied to one-half

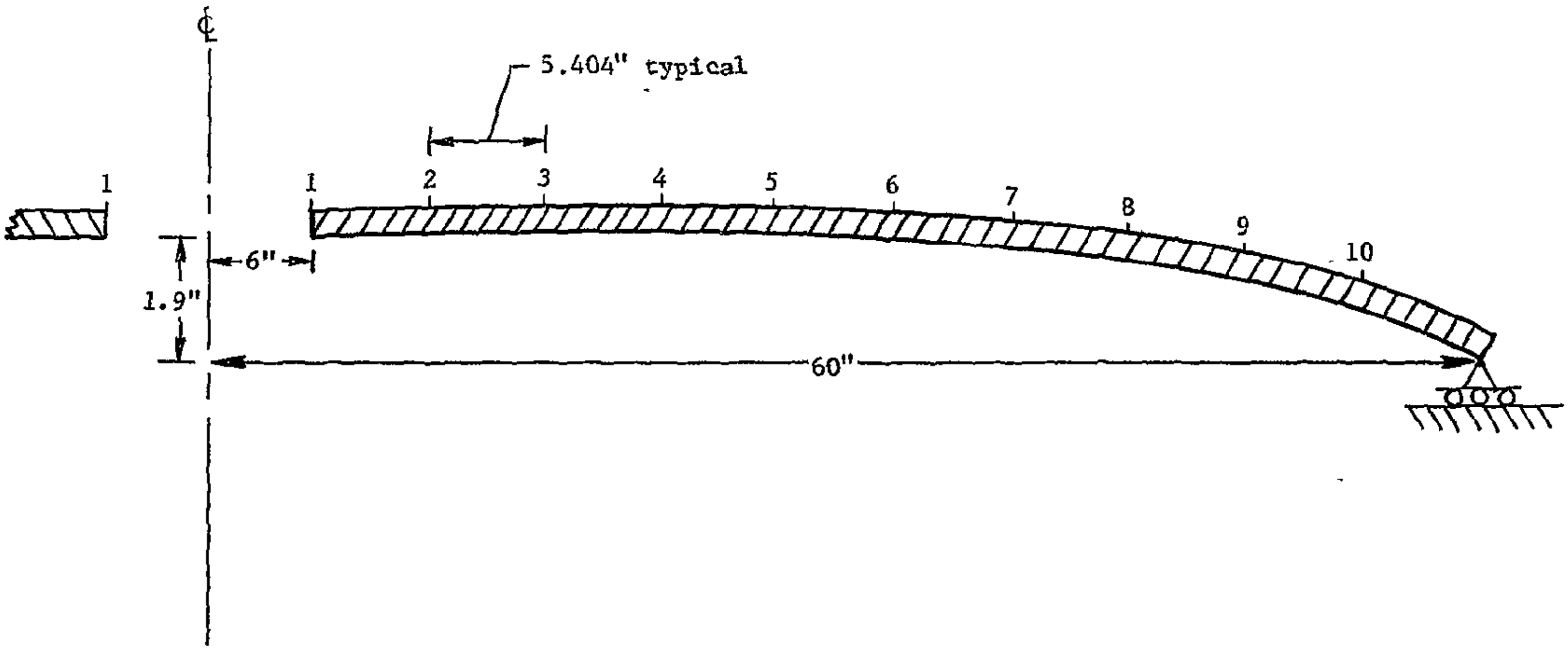

Figure 6.- Sketch of mirror cross section showing location of control points.

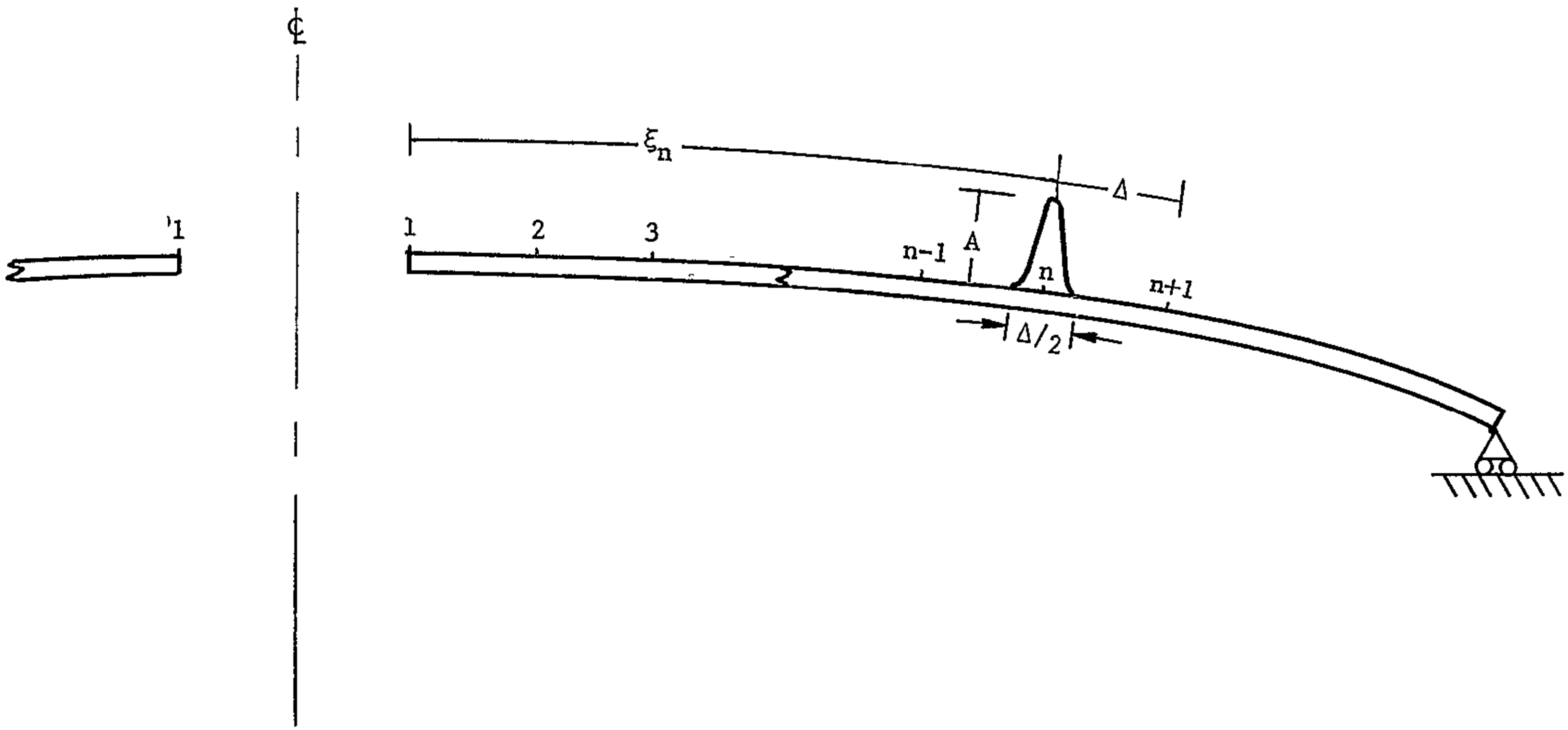

$$
T_n = \begin{cases} A\left[1/2 + 1/2\cos\dfrac{\pi\,(\xi - \xi_n)}{\Delta/4}\right] & |\xi - \xi_n| \leq \Delta/4 \\ 0 & |\xi - \xi_n| > \Delta/4 \end{cases}
$$

Figure 7.- Thermal inputs applied at control points along rear surface of mirror.

of the interval represented by the control point. This permits a spacing between the strip heaters.

The thermal inputs of Figure 7 were used at every control point except station 1 (see Fig. 6). At station 1 a slight modification of the thermal input was used. Only the right half of the distribution shown in Figure 7 was applied and the interior of the hole was assumed to be insulated.

Internal Temperature Distribution

The temperature distribution indicated in equation (5) was applied to the rear surface of the mirror at each control point. The application of this axially symmetric thermal input will result in two-dimensional heat flow within the mirror interior. Therefore, the interior temperature of the mirror (T_m) will be

$$T_m = T_m(\xi, \zeta) \tag{6}$$

where ξ is the meridional coordinate and ζ is the normal to the neutral surface. This temperature distribution must be determined in order to evaluate the effect of the thermal inputs in reducing mirror distortions. The internal temperature distribution could be significantly affected by the radiation heat loss from the mirror front surface. In order to evaluate the front surface heat loss at each control station, a thermal model of the telescope was examined. This model is shown in Figure 8. The mirror was represented by a flat circular disc. A disc was considered to be a good approximation because the mirror is

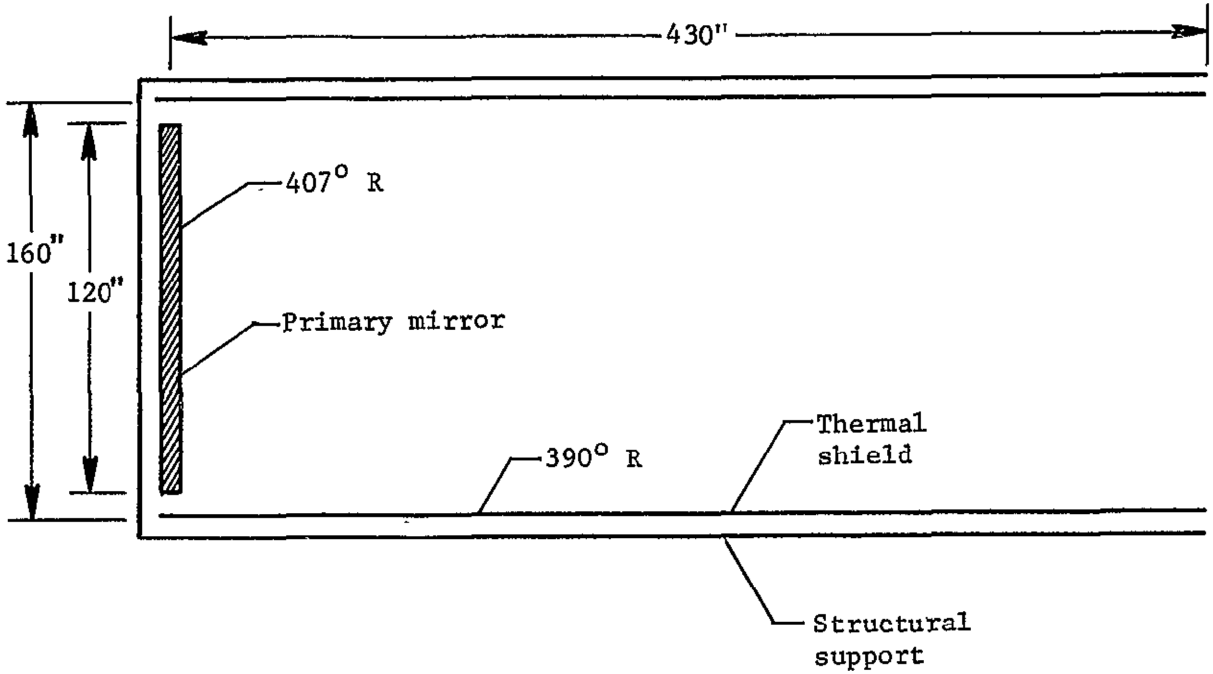

Figure 8.- Thermal model for calculation of axial heat loss.

a very shallow paraboloid with an edge to center depth of approximately 1.9 inches. The temperature of the mirror and thermal shield are 407° R and 390° R, respectively, and are assumed to be constant over the surface. These temperatures are based on a preliminary heat-transfer analysis reported in Reference 3. The interior of the thermal shield was coated with lampblack which has an emissivity of 0.96. The purpose of this coating is to eliminate stray radiation from falling on the telescope optics and introducing noise in the observations. Also, the secondary mirror and support struts were omitted from the model because the area was considered small.

The front surface radiation emitted by the mirror will be

$$Q_m = \sigma a_m A_m T_m^4 \tag{7}$$

where the emissivity and absorptivity are considered equal since the mirror and thermal shield are at approximately the same temperature. The mirror temperature is not considered to be significantly increased by the thermal inputs. The radiation from the thermal shield that strikes the mirror is

$$Q_{s\rightarrow m} = a_s \sigma T_s^4 A_s F_{sm} \tag{8}$$

where F_{sm} is the view factor and represents that portion of the energy emitted by the thermal shield which is intercepted by the mirror. Neglecting reflections, the net heat loss from the front surface of the mirror is equal to the radiation emitted by the mirror ($\sigma a_m A_m T_m^4$) minus the radiation absorbed by the mirror from the thermal

shield ($\sigma a_s T_s^4 A_s F_{sm} \cdot a_m$). This is expressed in equation form by the following relation:

$$Q = \sigma a_m A_m T_m^4 - \sigma a_s T_s^4 A_s F_{sm} a_m \tag{9}$$

In order to calculate the heat loss from the mirror it will be necessary to evaluate the view factor (F_{sm}) relating the radiant emission from the thermal shield which goes directly to the mirror. Since view factors are generally difficult to calculate due to involved integrals, simplifying relations are often sought. In order to determine the view factor between the thermal shield and mirror (F_{sm}), it will be related to the view factor between the mirror and open port (F_{mp}) which can be readily evaluated.

Since the mirror, heat shield, and opening at the end of the telescope (port) effectively form an enclosure and the disc does not radiate to itself,

$$F_{ms} + F_{mp} = 1 \tag{10}$$

Using this equation and the reciprocity relation

$$A_s F_{sm} = A_m F_{ms} \tag{11}$$

the view factor F_{sm} can be determined. By equation (11)

$$F_{sm} = \frac{A_m F_{ms}}{A_s} \tag{12}$$

Substituting for F_{ms} from equation (10)

$$F_{sm} = \frac{A_m(1 - F_{mp})}{A_s} \tag{13}$$

Replacing F_{sm} in equation (9) by equation (13) yields

$$Q = A_m \sigma a_m \left[T_m^4 - T_s^4 a_s (1 - F_{mp})\right] \tag{14}$$

In order to solve equation (14), it is necessary to determine the view factor F_{mp}. A sketch of the geometry is shown in Figure 9. From this sketch and the definition of the view factor (Ref. 9), we have

$$A_m F_{mp} = \int_{A_m} \int_{A_p} \frac{\cos \psi_m \cos \psi_p \, dA_p \, dA_m}{\pi b^2} \tag{15}$$

where

$$\cos \psi_m = \cos \psi_p = \frac{L}{b} \tag{16}$$

and

$$b = \sqrt{L^2 + (\rho_m - \rho_p)^2} \tag{17}$$

Substituting the above equations into equation (15) and also substituting for dA_p gives the following equation:

$$A_m F_{mp} = \int_{A_m} \int_0^{2\pi} \int_0^{80} \frac{L^2 \rho_p}{\pi \left[L^2 + (\rho_p - \rho_m)^2\right]^2} \, d\rho_p \, d\theta_p \, dA_m \tag{18}$$

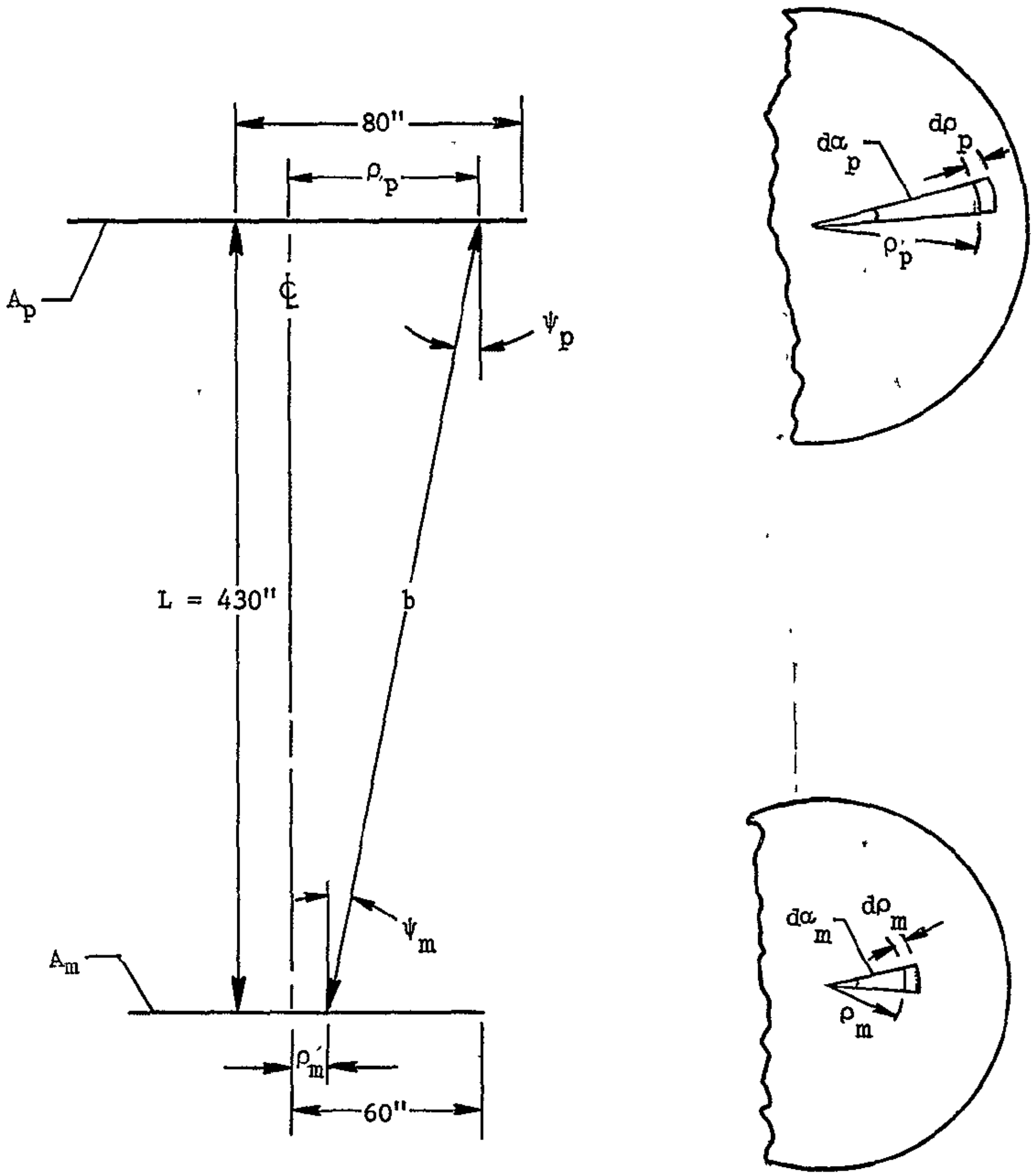

Figure 9.- Sketch of geometry to determine view factor.

Integrating this equation over $d\rho_p$ and $d\theta_p$ and substituting $L = 430$ in. yields the following integral over the mirror area:

$$A_m F_{mp} = \int_{A_m} \left\{ 1 - \frac{1.849 \times 10^5}{1.849 \times 10^5 + (80 - \rho_m)^2} + \frac{\rho_m(80 - \rho_m)}{1.849 \times 10^5 + (80 - \rho_m)^2} \right.$$

$$\left. + \frac{\rho_m}{430}\left[\tan^{-1}\left(\frac{80 - \rho_m}{430}\right) - \tan^{-1}\left(\frac{-\rho_m}{430}\right)\right] \right\} dA_m \tag{19}$$

Only the heat loss from the front surface at the control points is of interest. Each control point represents a small portion of the total mirror area. Therefore, since A_m is small in relation to A_p, equation (19) gives the view factor F_{mp} directly in terms of the mirror radius where it is to be evaluated. Therefore,

$$F_{mp} = 1 - \frac{1.849 \times 10^5}{1.849 \times 10^5 + (80 - \rho_m)^2} + \frac{\rho_m(80 - \rho_m)}{1.849 \times 10^5 + (80 - \rho_m)^2}$$

$$+ \frac{\rho_m}{430}\left[\tan^{-1}\left(\frac{80 - \rho_m}{430}\right) + \tan^{-1}\left(\frac{\rho_m}{430}\right)\right] \tag{20}$$

All terms necessary for evaluating the heat loss (eq. (14)) are now known. The calculated values for the view factor and the heat flux (Q/A_m) at each control point are shown in Table II. The view factors are quite small and do not vary significantly with the location of the control point. Since the heat flux is directly proportional to the view factor, it is also quite small.

The temperature gradient at the mirror surface can be determined using the Fourier heat conduction equation

$$-KA_m \frac{dT}{d\zeta} = Q \tag{21}$$

Simplifying this equation,

$$\frac{dT}{d\zeta} = - \frac{1}{K} \frac{Q}{A_m} \tag{22}$$

An examination of a typical temperature gradient (control point 5) indicates that

$$\frac{dT}{d\zeta} = 1.861 \times 10^{-4} \ {}^{o}R/in. \tag{23}$$

This is a small temperature gradient due to the view factor and the high thermal conductivity of beryllium. Since the temperature gradient at the mirror front surface is small, this boundary may be assumed to be insulated ($dT/d\zeta_{\zeta=t} = 0$) when determining the interior temperature distribution. Several nonmetallic materials, including ceramics and glasses, are also being considered for mirror fabrication. These materials have a very low thermal conductivity and therefore would have a larger temperature gradient at the mirror front surface.

The interior temperature distribution was examined by applying a thermal input of unit amplitude to the flat circular disc. A section view of the disc illustrating the coordinate system and thermal input

is shown in Figure 10. The thermal input is applied over the interval ρ_t. The front surface is thermally insulated due to the low-temperature gradient discussed previously. It should be noted that the conditions considered in this analysis are somewhat different from those shown in Figure 7. The thermal input is applied to the circular disc from the center outward, whereas the actual telescope would have the central portion removed. The solid disc was chosen because it should have little effect on the internal temperature distribution and the finiteness condition at the center (discussed later) readily permits evaluation of constants necessary for the solution of the differential equation.

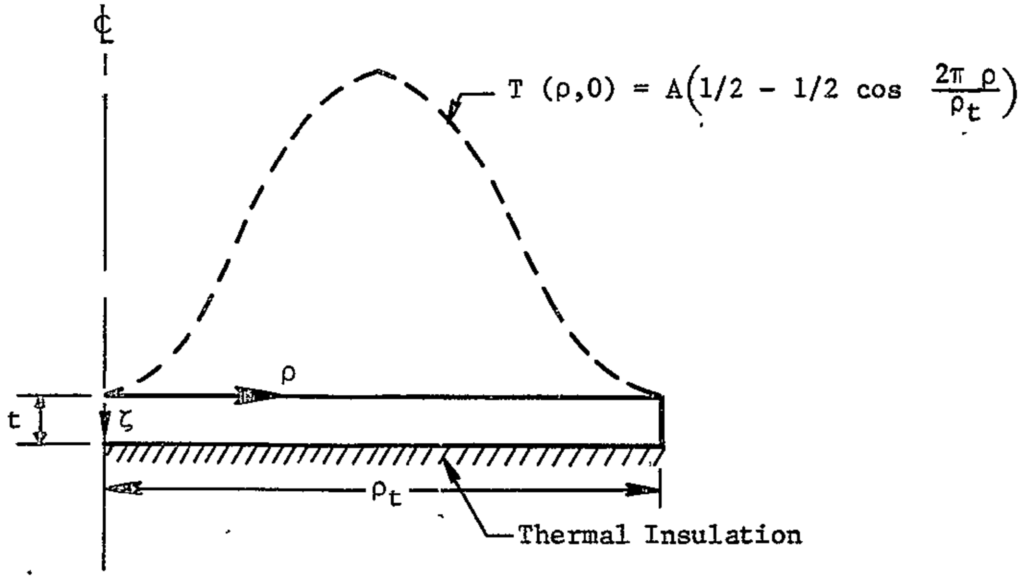

Figure 10.- Sketch illustrating the coordinate system and boundary conditions for determining the temperature distribution in a circular disc.

The general differential equation for an axisymmetric steady-state temperature distribution in a circular disc is given below (Ref. 10):

$$\frac{\partial^2 T}{\partial \rho^2} + \frac{1}{\rho}\frac{\partial T}{\partial \rho} + \frac{\partial^2 T}{\partial \zeta^2} = 0 \tag{24}$$

The boundary and finiteness conditions applicable to this problem are

$$T(0,\zeta) \qquad \text{is finite} \tag{25}$$

$$\left.\frac{\partial T}{\partial \zeta}\right|_{\zeta=t} = 0 \qquad \text{insulated front surface} \tag{26}$$

$$T(\rho,0) = A\left(\frac{1}{2} - \frac{1}{2}\cos\frac{2\pi\rho}{\rho_t}\right) \tag{27}$$

Therefore,

$$\left.\frac{\partial T}{\partial \rho}\right|_{\rho=\rho_t} = 0 \tag{28}$$

The finiteness condition (eq. (25)) results from physical limitations on the temperature at the center of the disc. It was noted that the disc was chosen instead of an annular ring because the finiteness condition simplifies the solution without significantly modifying the problem. The second boundary condition (eq. (26)) has been discussed previously. Equation (28) can be shown directly from the imposed temperature distribution given as equation (27). The equation for the applied distribution (eq. (27)) is different from equation (5); however,

the actual thermal input is the same. The governing differential equation (eq. (24)) can be solved by the separation of variables technique. Assume a product solution of the form

$$T(\rho,\zeta) = R(\rho)Z(\zeta) \tag{29}$$

Substituting equation (29) into equation (24) and performing the indicated differentiation yields the relation

$$\frac{1}{R}\frac{\partial^2 R}{\partial \rho^2} + \frac{1}{R\rho}\frac{\partial R}{\partial \rho} = -\frac{1}{Z}\frac{\partial^2 Z}{\partial \zeta^2} \tag{30}$$

Since the left-hand portion of the equation is independent of ζ and the equivalent right-hand member is independent of ρ, both sides must therefore be independent of ζ and ρ and may be set equal to a constant $-\lambda^2$.

$$\frac{1}{R}\frac{\partial^2 R}{\partial \rho^2} + \frac{1}{R\rho}\frac{\partial R}{\partial \rho} = -\lambda^2 \tag{31}$$

$$\frac{1}{Z}\frac{\partial^2 Z}{\partial \zeta^2} = \lambda^2 \tag{32}$$

Equation (31) is a Bessels equation. The solution to this equation is a Bessels function of the second kind of order zero. Equation (32) is an ordinary linear differential equation whose solution may be obtained using operator techniques. The solutions to both equations are given in equations (33) and (34), respectively.

$$R = C_1 J_o(\lambda\rho) + C_2 Y_o(\lambda\rho) \tag{33}$$

$$Z = C_3\ e^{\lambda\zeta} + C_4\ e^{-\lambda\zeta} \tag{34}$$

The temperature may now be determined from the product of equations (33) and (34).

$$T = R(\rho)Z(\zeta) = \left[C_1 J_o(\lambda\rho) + C_2 Y_o(\lambda\rho)\right]\left[C_3\ e^{\lambda\zeta} + C_4\ e^{-\lambda\zeta}\right] \tag{35}$$

The constants will be determined by imposing the boundary and finiteness conditions. The first condition requires that $C_2 = 0$ because the $\underset{\rho \to 0}{\text{limit}}\ Y_o(\lambda\rho) \to \infty$. Redefining and combining constants, the temperature may be expressed as

$$T = \left[C_1\ e^{\lambda\zeta} + C_2\ e^{-\lambda\zeta}\right] J_o(\lambda\rho) \tag{36}$$

Partial differentiation of equation (36) with respect to ζ and imposing the boundary condition of equation (26) yields the following relation between constants C_1 and C_2 where t denotes the mirror thickness.

$$C_1 = C_2\ e^{-2\lambda t} \tag{37}$$

Therefore,

$$T = C_2 J_o(\lambda\rho)\left[e^{\lambda\zeta - 2\lambda t} + e^{-\lambda\zeta}\right] \tag{38}$$

The separation constant λ may be defined by the fourth boundary condition given in equation (28).

$$\left.\frac{\partial T}{\partial \rho}\right|_{\rho=\rho_t} = -C_2\lambda J_1(\lambda\rho_t)\left[e^{\lambda\zeta-2\lambda t} + e^{-\lambda\zeta}\right] = 0 \tag{39}$$

The only way this equation may be satisfied without having a trivial solution is for

$$\lambda J_1(\lambda\rho_t) = 0 \tag{40}$$

which yields the following first four values for λ:

$$\left.\begin{aligned} \lambda_o &= 0 \\ \lambda_1 &= \frac{3.8317}{\rho_t} \\ \lambda_2 &= \frac{7.0156}{\rho_t} \\ \lambda_3 &= \frac{10.173}{\rho_t} \end{aligned}\right\} \tag{41}$$

The general solution of the equation must involve the sum over all λ and may be written as

$$T = 2C_o + \sum_{n=1}^{\infty} C_n J_o(\lambda_n\rho)\left[e^{\lambda_n\zeta-2\lambda_n t} + e^{-\lambda_n\zeta}\right] \tag{42}$$

The above equation specifies the interior temperature distribution of a flat circular disc with the front surface insulated against heat losses. The relation is complete except for determining the constant C which

may be defined using the imposed temperature distribution. By examining the distribution over the interval from 0 to ρ_t and noting the orthogonality relation, the constants can be determined from equations defined in Reference 11. From the reference, the constants are

$$C_o = \frac{1}{\rho_t^2} \int_o^{\rho_t} \rho T(\rho,0) d\rho \tag{43}$$

$$C_n = \frac{1}{B_n(1 + e^{-2\lambda_n t})} \int_o^{\rho_t} \rho T(\rho,0) J_o(\lambda_n \rho) d\rho \tag{44}$$

$$B_n = \int_o^{\rho_t} \rho \left[J_o(\lambda_n \rho)\right]^2 d\rho \tag{45}$$

where $n = 1,2,3,4,\ldots,\infty$.

Substituting $A\left(\frac{1}{2} - \frac{1}{2}\cos\frac{2\pi\rho}{\rho_t}\right)$ for $T(\rho,0)$ into the equation for C_o, that constant can be found to be

$$C_o = \frac{A}{4} \tag{46}$$

Performing the same substitution, C_n may be found to be

$$C_n = -\frac{A}{2B_n(1 + e^{-2\lambda_n t})} \int_o^{\rho_t} \rho \left(\cos\frac{2\pi\rho}{\rho_t}\right) J_o(\lambda_n \rho) d\rho \tag{47}$$

where B_n is given in Reference 11 as

$$B_n = \frac{p_t^2}{2}\left[J_o(\lambda_n \rho_t)\right]^2 \tag{48}$$

Therefore, substituting C_o into equation (42) and B_n into equation (47), we have

$$T = \frac{A}{2} + \sum_{n=1}^{\infty} C_n J_o(\lambda_n \rho)\left[e^{\lambda_n(\zeta - 2t)} + e^{-\lambda_n \zeta}\right] \tag{49}$$

$$C_n = \frac{-A}{\rho_t^{\,2}\left[J_o(\lambda_n \rho_t)\right]^2\left[1 + e^{-2\lambda_n t}\right]} \int_o^{\rho_t} \rho \left[\cos \frac{2\pi\rho}{\rho_t}\right] J_o(\lambda_n \rho)\, d\rho \tag{50}$$

The integral in equation (50) for C_n cannot be evaluated directly but must be found graphically or numerically for each value of λ_n. A computer program to evaluate both equations (49) and (50) was written in the Fortran 2.3 programing language and is included in Appendix A. The Gauss quatrature method was used to evaluate the integral in equation (50). The computer program was utilized to determine the difference between the applied back surface temperature and the temperature of the interior as a function of radius. The first 20 terms in the series of equation (49) were used.

The results of these calculations for a unit amplitude indicate that the maximum temperature difference is 0.016° and occurs along the axis of the disc. The temperature difference as a function of radius for $\zeta = 0.5$ and $\zeta = 1.0$ is shown in Figure 11. It should be noted that the maximum temperature difference does not occur at the same location as the maximum thermal input.

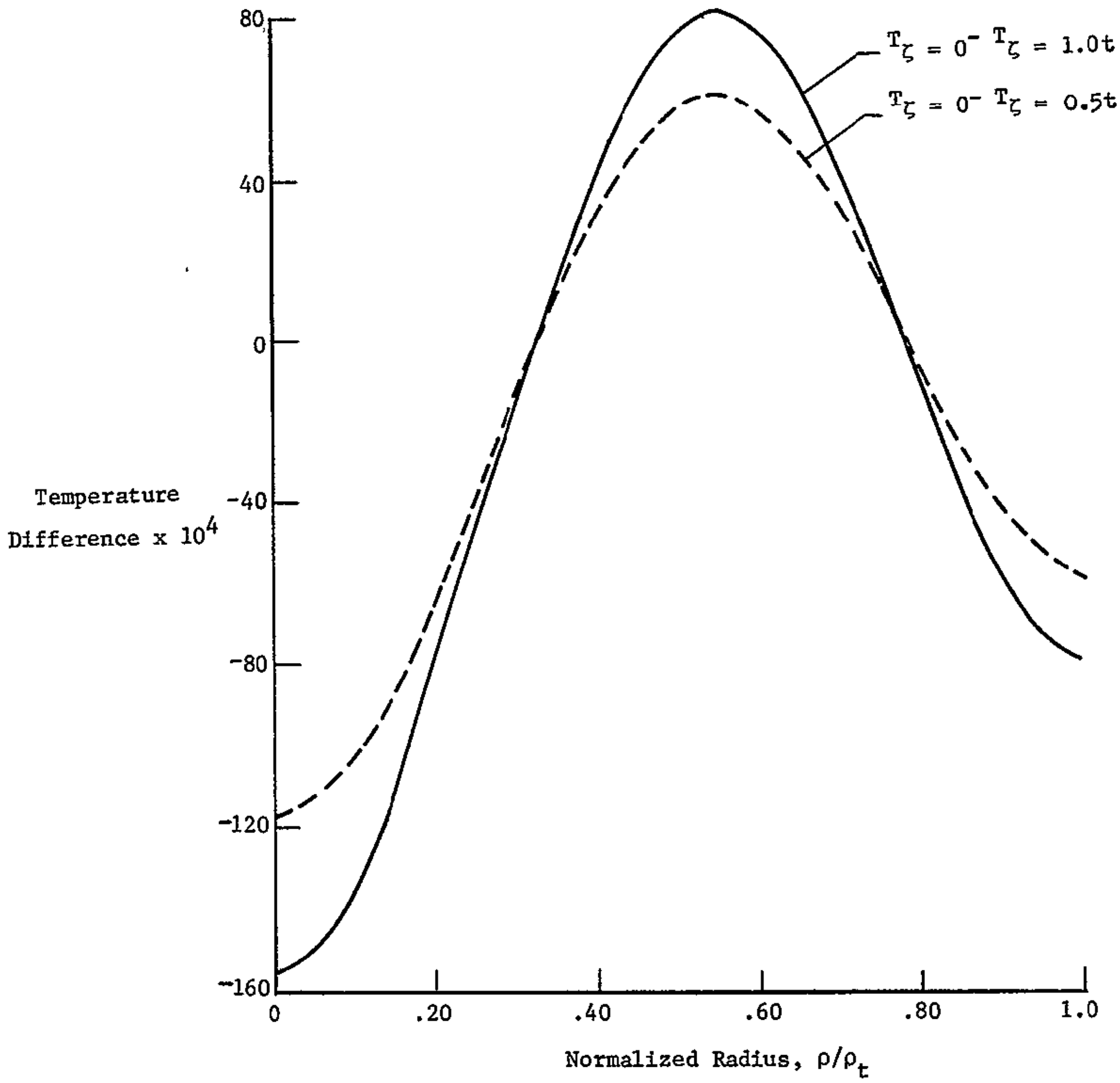

Figure 11.- Temperature difference through a circular disc as a function of radius.

CHAPTER IV

THERMAL INFLUENCE COEFFICIENTS

Paraboloid of Revolution

The distortion influence coefficients relating the thermal input and the distortion at the control points will now be determined. Several techniques for determining these coefficients are available. One method which has been employed for the force active optics system is the finite element technique (Ref. 12). This technique consists of dividing the mirror into small interconnected elements of finite size. The deformations of the mirror are determined at the points of connection called nodes. The method used in the present investigation is the finite difference technique in which the governing differential equations are solved by approximating the derivatives by finite differences between nodes. Either technique may be used to determine the deflection influence coefficients. Once the deflection influence coefficients (c_{ij} in eq. (1)) have been evaluated, a flexibility matrix for the control points can be formulated. The amplitude of the thermal inputs necessary to correct mirror distortions can be expressed by inverting the flexibility matrix.

The equations governing the linear behavior of thin shells of revolution are well known and may be found in References 13 and 14. The basic equations will be shown here to clarify this analysis. The mirror was considered to be fabricated from a homogeneous and isotropic material and only static symmetrical distortions are of interest. The

geometry and coordinate system for a paraboloidal shell are shown in Figure 12. Any point in the shell may be located by specifying its coordinates (ξ,θ,ζ). The origin and positive direction of the coordinates are indicated on the figure. The meridional coordinate is denoted as ξ, the circumferential coordinate as θ, and the normal to the tangent plane is indicated as ζ. The neutral surface is chosen so that

$$\int \zeta E \, d\zeta = 0 \tag{51}$$

where the integration is through the thickness. This permits a variation in the modulus due to temperature changes to be considered. The modulus of the beryllium used in this analysis was considered to be constant; therefore, the neutral surface will be the middle surface of the shell. The principal radii of curvature R_θ and R_ξ are written in terms of ρ and ξ as

$$R_\theta = \frac{\rho}{\sqrt{1 - \left(\frac{d\rho}{d\xi}\right)^2}} \tag{52}$$

$$R_\xi = - \frac{\sqrt{1 - \left(\frac{d\rho}{d\xi}\right)^2}}{\left(\frac{d^2\rho}{d\xi^2}\right)} \tag{53}$$

These relationships can be defined using the usual parabolic relationship between the radial and axial coordinates.

$$\rho^2 = 4fy \tag{54}$$

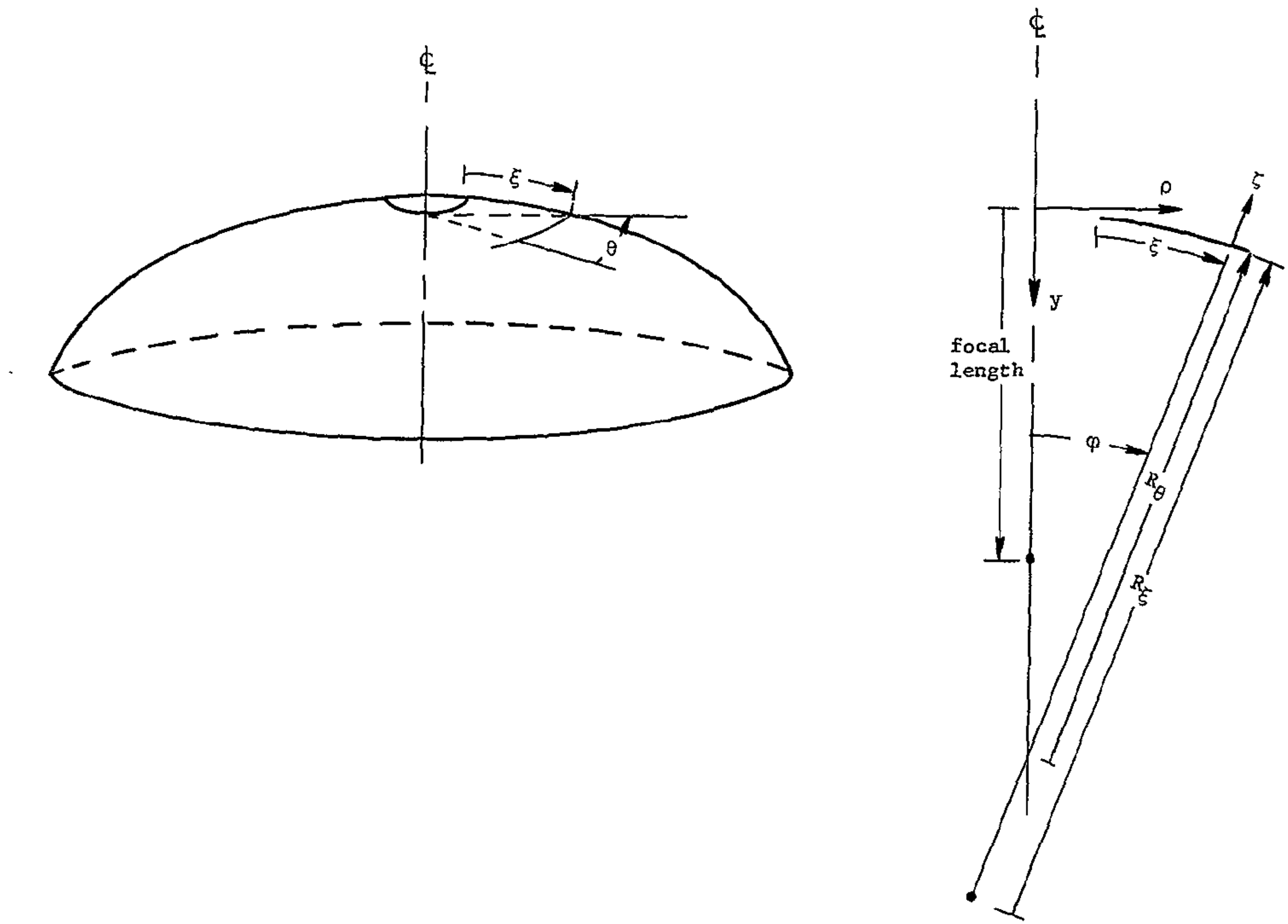

Figure 12.- Paraboloidal surface geometry and coordinate system.

Utilizing the definition for the length of a differential element

$$d\xi = \sqrt{d\rho^2 + dy^2} \tag{55}$$

we can obtain

$$\frac{d\rho}{d\xi} = \frac{1}{\sqrt{\left(\frac{\rho^2}{4f^2}\right) + 1}} \tag{56}$$

from which the radii of curvature can be shown to be

$$R_\theta = \sqrt{4f^2 + \rho^2} \tag{57}$$

$$R_\xi = \left(\frac{1}{4f^2}\right) \times (4f^2 + \rho^2)^{3/2} \tag{58}$$

A shell element indicating the positive directions of the membrane forces per unit length, transverse forces per unit length, and loading per unit area is shown in Figure 13(a). The moments per unit length are given in Figure 13(b) and the positive directions of displacement and rotation are shown in Figure 14. The equilibrium equations for any isotropic shell of revolution loaded axisymmetrically are shown below (Ref. 15).

$$\left.\begin{aligned} &\frac{\partial \rho N_\xi}{\partial \xi} - N_\theta \frac{\partial \rho}{\partial \xi} + \frac{1}{R_\xi}\left(\frac{\partial \rho M_\xi}{\partial \xi} - M_\theta \frac{\partial \rho}{\partial \xi}\right) + \rho q_\xi = 0 \\ &\frac{\partial}{\partial \xi}\left(\frac{\partial \rho M_\xi}{\partial \xi} - M_\theta \frac{\partial \rho}{\partial \xi}\right) - \rho\left(\frac{N_\xi}{R_\xi} + \frac{N_\theta}{R_\theta}\right) + \rho q = 0 \end{aligned}\right\} \tag{59}$$

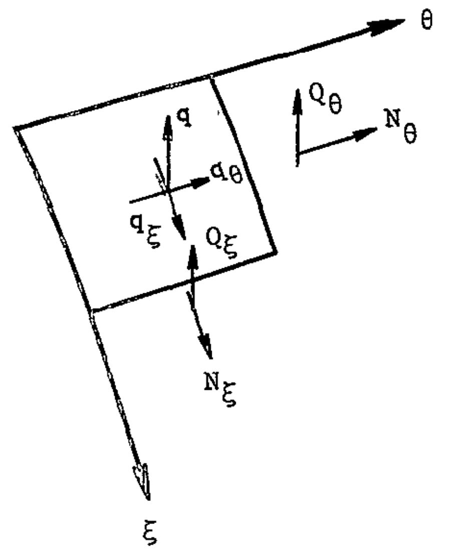

(a) Stress resultants and loads.

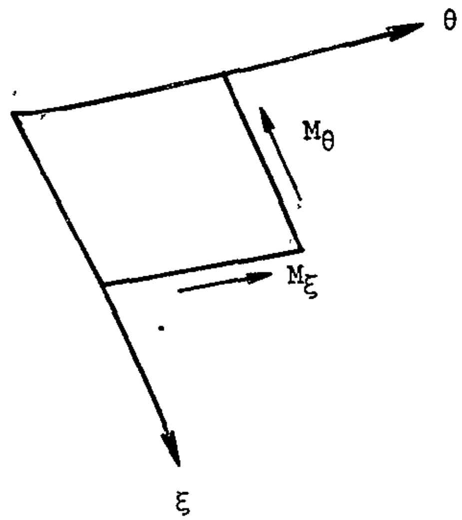

(b) Moment resultants.

Figure 13.- Shell element with stress resultants, stress moments, and loads applied in the positive sense.

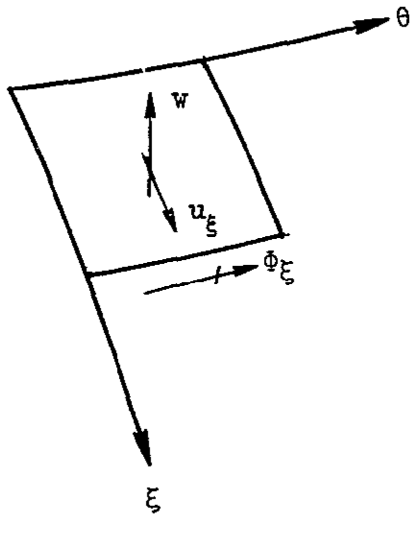

Figure 14.- Shell element with displacements and rotation indicated in the positive sense.

The transverse shear forces have been eliminated by using the moment equilibrium equations.

The displacements and rotation of the midplane surface are related by

$$\Phi_\xi = -\frac{\partial w}{\partial \xi} + \frac{u_\xi}{R_\xi} \tag{60}$$

The membrane strains are expressed in terms of displacements by

$$\left.\begin{aligned} \epsilon_\xi &= \frac{\partial u_\xi}{\partial \xi} + \frac{w}{R_\xi} \\ \epsilon_\theta &= \frac{u_\xi}{\rho}\frac{\partial \rho}{\partial \xi} + \frac{w}{R_\xi} \end{aligned}\right\} \tag{61}$$

The distortions due to bending are given by

$$\left.\begin{aligned} K_\xi &= \frac{\partial \Phi_\xi}{\partial \xi} \\ K_\theta &= \frac{\Phi_\xi}{\rho}\frac{\partial \rho}{\partial \xi} \end{aligned}\right\} \tag{62}$$

Neglecting the effects of stresses normal to the shell and assuming surface normals to the neutral surface remain normal after deformation, the stress-strain relations are given by the following equations:

$$\left.\begin{aligned} \epsilon_\xi + \zeta K_\xi &= \frac{\sigma_\xi - \nu\sigma_\theta}{E} + \alpha T \\ \epsilon_\theta + \zeta K_\theta &= \frac{\sigma_\theta - \nu\sigma_\xi}{E} + \alpha T \end{aligned}\right\} \tag{63}$$

The stress-strain relations along with the definition of the stress and moment resultants

$$\left.\begin{aligned} N_\xi &= \int \sigma_\xi \, d\zeta & \qquad M_\xi &= \int \zeta\sigma_\xi \, d\zeta \\ N_\theta &= \int \sigma_\theta \, d\zeta & \qquad M_\theta &= \int \zeta\sigma_\theta \, d\zeta \end{aligned}\right\} \tag{64}$$

and the relation

$$\int \zeta E \, d\zeta = 0 \tag{51}$$

yield the following relations:

$$\left.\begin{aligned} \epsilon_\xi &= \frac{N_\xi - \nu N_\theta + \int E\alpha T \, d\zeta}{\int E \, d\zeta} \\ \epsilon_\theta &= \frac{N_\theta - \nu N_\xi + \int E\alpha T \, d\zeta}{\int E \, d\zeta} \\ K_\xi &= \frac{M_\xi - \nu M_\theta + \int \zeta E\alpha T \, d\zeta}{\int \zeta^2 E \, d\zeta} \\ K_\theta &= \frac{M_\theta - \nu M_\xi + \int \zeta E\alpha T \, d\zeta}{\int \zeta^2 E \, d\zeta} \end{aligned}\right\} \tag{65}$$

Equations (59) - (62) and (65) constitute a set of 11 equations relating 11 independent variables. By combining these equations, a set of three second-order differential equations in terms of meridional and axial displacements (u_ξ and w) and meridional moment resultant (M_ξ) can be obtained.

The three second-order differential equations are subject to restraints applied along the boundary of the shell. The boundary conditions and mirror support system were discussed previously and are shown in Figure 5. The periphery of the shell will not support a moment M_ξ due to the hinge. The sum of forces in the radial direction equals zero, as do the axial displacements. The positive direction of forces and displacements at the outer boundary are shown in Figure 15(a). The equations used in describing this boundary condition are as follows:

$$\left.\begin{aligned} &M_\xi = 0 \\ &w \cos \varphi - u_\xi \sin \varphi = 0 \\ &Q_\xi \sin \varphi + N_\xi \cos \varphi = 0 \end{aligned}\right\} \tag{66}$$

The central cutout portion of the mirror was unrestrained. Therefore, no resultant forces or moments can be accommodated at this boundary. The positive direction of forces and displacements at the inner boundary are shown in Figure 15(b). The equations used to describe this boundary condition are as follows:

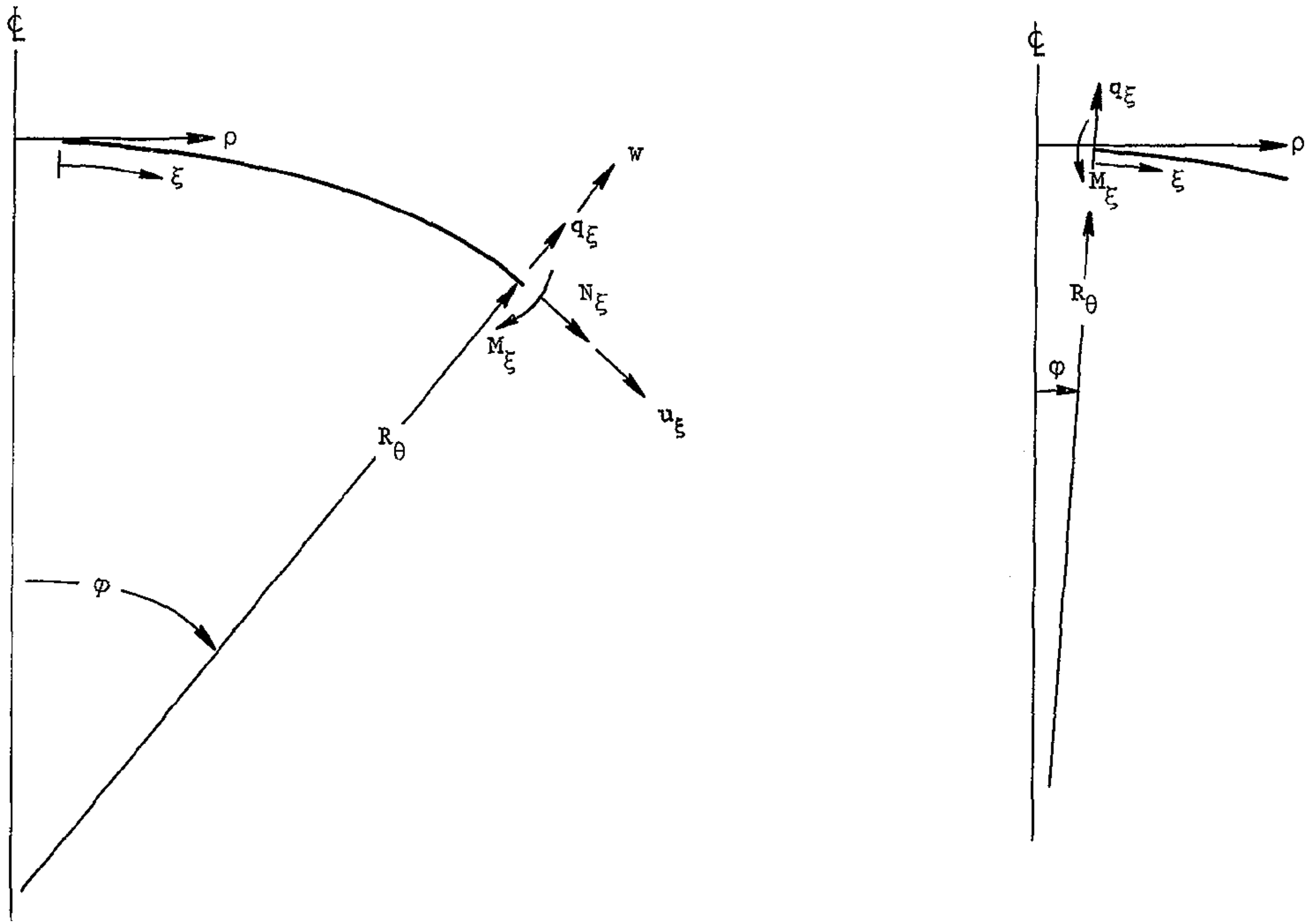

a. Outer boundary   b. Inner boundary

Figure 15.- Sketch illustrating the positive direction of the forces and displacements at the boundary.

$$\left.\begin{aligned} M_\xi &= 0 \\ N_\xi &= 0 \\ Q_\xi &= 0 \end{aligned}\right\} \tag{67}$$

As noted previously, diffraction-limited operation of a telescope mirror requires that axial distortions of the primary mirror be kept within a tolerance limit of 2 microinches. The relation between axial distortions and the distortions along the shell meridian and normal to the shell meridian may be seen in Figure 16. These distortions are related by the equation

$$\delta = w \cos \varphi - u_\xi \sin \varphi \tag{68}$$

Therefore, the axial distortion at any point is directly related by the coordinates of the point and the deformation of the shell meridian. One finite difference solution for the linear behavior of shells of revolution has been programed by Schaeffer for the digital computer and is presented in Reference 16. Using this program, a digital computer will calculate stress and moment resultants and displacements for thermal and force loading varying along the meridian of the shell.

Distributed Thermal Inputs

An analytical model of the telescope mirror was developed using the finite difference solution of the shells equations from Reference 16. Utilizing this analysis, the distortions due to the application of a unit thermal input at the control point of interest was determined.

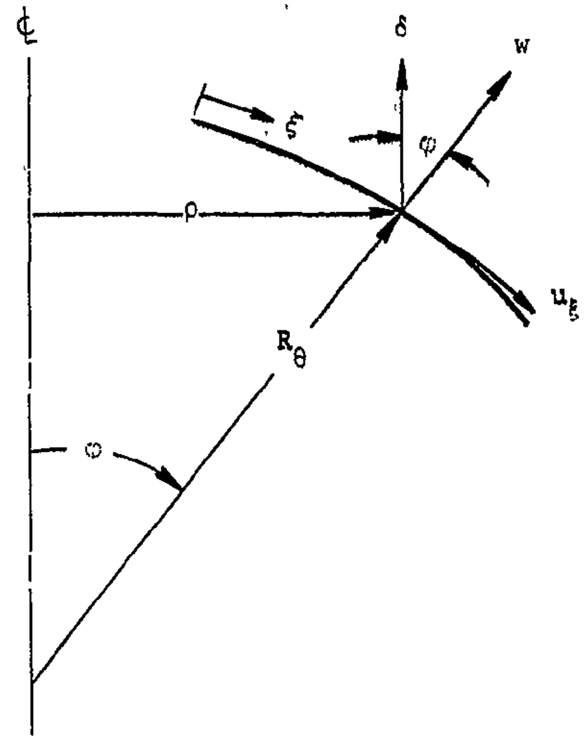

Figure 16.- Sketch showing axial shell distortion.

Thermal inputs at all other control points were zero. This is shown below in equation form.

$$
\left.
\begin{aligned}
\delta_1 &= c_{11}T_1 + c_{12}T_2 + c_{13}T_3 + \cdots c_{1n}T_n \\
\delta_2 &= c_{21}T_1 + c_{22}T_2 + c_{23}T_3 + \cdots c_{2n}T_n \\
\delta_3 &= c_{31}T_1 + c_{32}T_3 + c_{33}T_3 + \cdots c_{3n}T_n \\
&\ \vdots \\
\delta_n &= c_{n1}T_1 + c_{n2}T_2 + c_{n3}T_3 + \cdots c_{nn}T_n
\end{aligned}
\right\} \qquad (1)
$$

Assume the control point of interest is number 1. If we assign T_1 an amplitude $A = 1$ and $T_2, T_3, \ldots, T_n$ an amplitude $A = 0$, then

$$\left.\begin{aligned} \delta_1 &= c_{11} \\ \delta_2 &= c_{21} \\ \delta_3 &= c_{31} \\ &\vdots \\ \delta_n &= c_{n1} \end{aligned}\right\} \qquad (69)$$

By applying a unit amplitude at each control point separately, each column of coefficients may be determined.

The analytical model used in this analysis has the capability of accommodating 502 control points along the shell meridian. A large number of control points is desirable because it increases the accuracy of the active optics system. However, since the flexibility matrix must be inverted in order to determine the stiffness matrix, the number of stations may be limited by the inversion routine. The inversion of large matrices is time consuming even for the best digital computers available. The accuracy of the inversion is limited by the behavior of the original matrix. One way to avoid this is to allow the thermal input to span several points in the finite difference analysis. The midpoint of the thermal input may be selected as the control point for correction by the figure error sensor in the active control system. The thermal inputs necessary for the correction of any given distortion

is therefore the amplitude (A) of the same distribution used to determine the flexibility matrix.

Structures subjected to concentrated force loading have symmetrical flexibility matrices. Linear transformations with real symmetric matrices dominate the study of deformations of elastic media. Therefore, it is of interest to examine the flexibility matrix formed by distributed thermal inputs. Matrices generated by concentrated force loads are symmetrical because of the reciprocity theorem. This theorem states that for linear structures a force F_i acting through a displacement caused by force F_j does the same amount of work as force F_j acting through a displacement caused by force F_i. This can be expressed in equation form as

$$F_i(c_{ij}F_j) = F_j(c_{ji}F_i) \tag{70}$$

and, therefore,

$$c_{ij} = c_{ji} \tag{71}$$

Since the coefficients of the flexibility matrix form a symmetrical array, the inverse or stiffness matrix must also be symmetrical. The basis of the reciprocity theorem lies in the fact that the total energy stored in an elastic system is independent of the order in which the loads are applied. This is also true of elastic systems deformed by thermal inputs. Therefore, the systems are analogous and for concentrated thermal loads the flexibility and stiffness matrices are symmetric.

For distributed thermal inputs, however, the flexibility matrix may not be symmetric. In order to examine the flexibility matrix formed by distributed loads, we will now examine the case for a simply supported beam. A continuous beam with concentrated loads applied along three control points is shown in Figure 17(a). The deformation at any station along the beam may be determined from the following equations:

$$\begin{Bmatrix} \delta_1 \\ \delta_2 \\ \delta_3 \\ \cdot \\ \cdot \\ \cdot \\ \delta_n \end{Bmatrix} = \begin{bmatrix} c_{11} & c_{12} & c_{13} & c_{14} & \cdots & c_{1n} \\ c_{21} & c_{22} & c_{23} & c_{24} & \cdots & c_{2n} \\ c_{31} & c_{32} & c_{33} & c_{34} & \cdots & c_{3n} \\ & & & & & \\ & & & & & \\ c_{n1} & c_{n2} & c_{n3} & c_{n4} & \cdots & c_{nn} \end{bmatrix} \begin{Bmatrix} T_1 \\ T_2 \\ T_3 \\ \\ \\ \\ T_n \end{Bmatrix} \tag{72}$$

If only the deformations under the loads are of interest, the equation can be simplified to (since T_1, T_3, T_4, etc. = 0)

$$\begin{Bmatrix} \delta_2 \\ \delta_5 \\ \delta_8 \end{Bmatrix} = \begin{bmatrix} c_{22} & c_{25} & c_{28} \\ c_{52} & c_{55} & c_{58} \\ c_{82} & c_{85} & c_{88} \end{bmatrix} \begin{Bmatrix} T_2 \\ T_5 \\ T_8 \end{Bmatrix} \tag{73}$$

The application of a distributed load of unit amplitude on the same beam wide enough to cover several stations is shown in Figure 17(b). The deformations at control points 2, 5, and 8 due to the distributed load at stations 1, 2, and 3 are

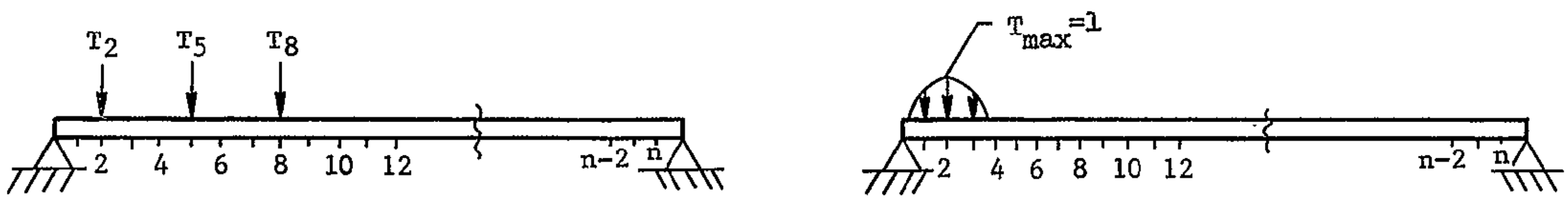

a. Beam with concentrated loads

b. Beam with distributed loads

Figure 17.- Sketch illustrating elastic beam with applied loading.

$$\left.\begin{aligned}\delta_2 &= c_{21}(K) + c_{22}(1) + c_{23}(K)\\ \delta_5 &= c_{51}(K) + c_{52}(1) + c_{53}(K)\\ \delta_8 &= c_{81}(K) + c_{82}(1) + c_{83}(K)\end{aligned}\right\} \tag{74}$$

where K is a constant less than 1. If a distributed load of this form is always applied, the amplitude of the distribution may be denoted as $\bar{T}$. If the deformations at points 2, 5, and 8 are the only control points of interest, a new equation may be written as follows:

$$\begin{Bmatrix}\delta_2\\ \delta_5\\ \delta_8\end{Bmatrix} = \begin{bmatrix}[c_{21}(K) + c_{22}(1) + c_{23}(K)] & [\qquad] & [\qquad]\\ [c_{51}(K) + c_{52}(1) + c_{53}(K)] & [\qquad] & [\qquad]\\ [c_{81}(K) + c_{82}(1) + c_{83}(K)] & [\qquad] & [\qquad]\end{bmatrix}\begin{Bmatrix}\bar{T}_2\\ \bar{T}_5\\ \bar{T}_8\end{Bmatrix} \tag{75}$$

The second column of coefficients for control point 5 due to the same load applied at stations 4, 5, and 6 is shown in the following equation:

$$\begin{Bmatrix}\delta_2\\ \delta_5\\ \delta_8\end{Bmatrix} = \begin{bmatrix}[c_{21}(K) + c_{22}(1) + c_{23}(K)] & [c_{24}(K) + c_{25}(1) + c_{26}(K)] & [\qquad]\\ [c_{51}(K) + c_{52}(1) + c_{53}(K)] & [c_{54}(K) + c_{55}(1) + c_{56}(K)] & [\qquad]\\ [c_{81}(K) + c_{82}(1) + c_{83}(K)] & [c_{84}(K) + c_{85}(1) + c_{86}(K)] & [\qquad]\end{bmatrix}\begin{Bmatrix}\bar{T}_2\\ \bar{T}_5\\ \bar{T}_8\end{Bmatrix} \tag{75}$$

The above equation indicates that the matrix of coefficients for the distributed load is not symmetrical. For example,

$$c_{51}(K) + c_{52}(1) + c_{53}(K) \neq c_{24}(K) + c_{25}(1) + c_{26}(K) \tag{76}$$

because even though

$$c_{52} = c_{25} \tag{77}$$

the remaining coefficients

$$c_{51} + c_{53} \neq c_{24} + c_{26} \tag{78}$$

are not necessarily equal.

CHAPTER V

RESULTS AND DISCUSSION

The thermal influence coefficients for the primary telescope mirror were determined using the computerized finite difference solution of the elastic shells equations. Ten control points equally spaced along the meridian of the primary telescope mirror were selected. The thermal inputs were considered to be applied by sources with controlled temperature distributions located on the back surface of the mirror. The thermal gradients in the interior of the mirror were neglected since they were shown previously to be quite small.

The axial distortion due to the application of each symmetrical thermal input is shown in Figure 18. These curves illustrate the distortion due to the application of a thermal input of unit amplitude at each control point. The location of each control point is indicated on the figure. The distortions are a maximum at the inner unrestrained boundary (except for control point 7) and decrease uniformly to zero at the axially restrained outer boundary. Maximum distortion is obtained by thermal inputs located at control points 4 and 10. It was noted previously that mirror distortions must be maintained to within 2 microinches in order for the telescope to operate at the diffraction limit. The distortion created by a unit thermal input at control point 10 is over 300 times the allowable level. The large change in distortion between control points 9 and 10 as opposed to the relatively small change for points 3 and 4 indicates that this arrangement of

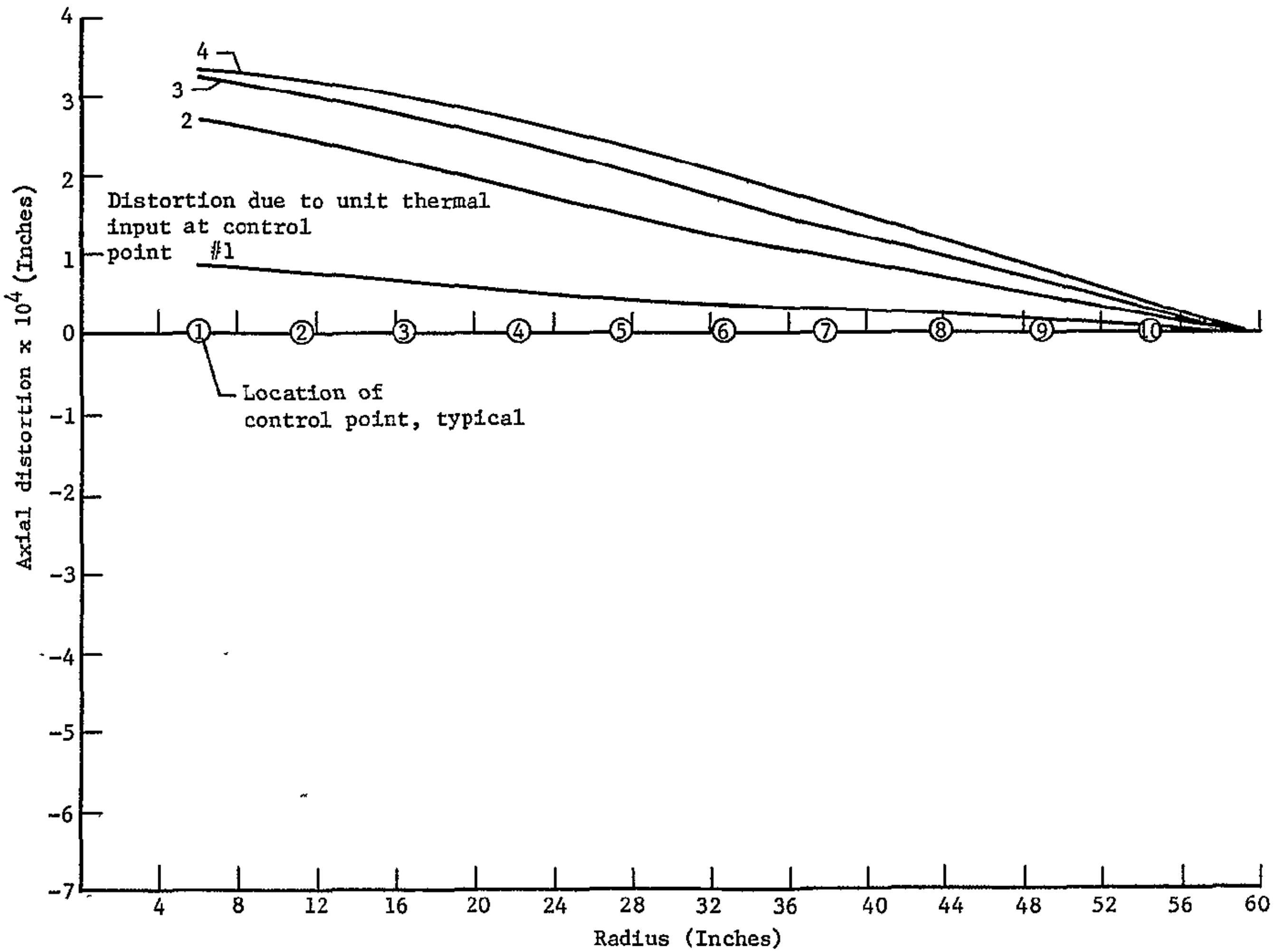

a. Thermal input applied individually at control points 1 - 4.

Figure 18.- Axial distortion due to applied thermal input.

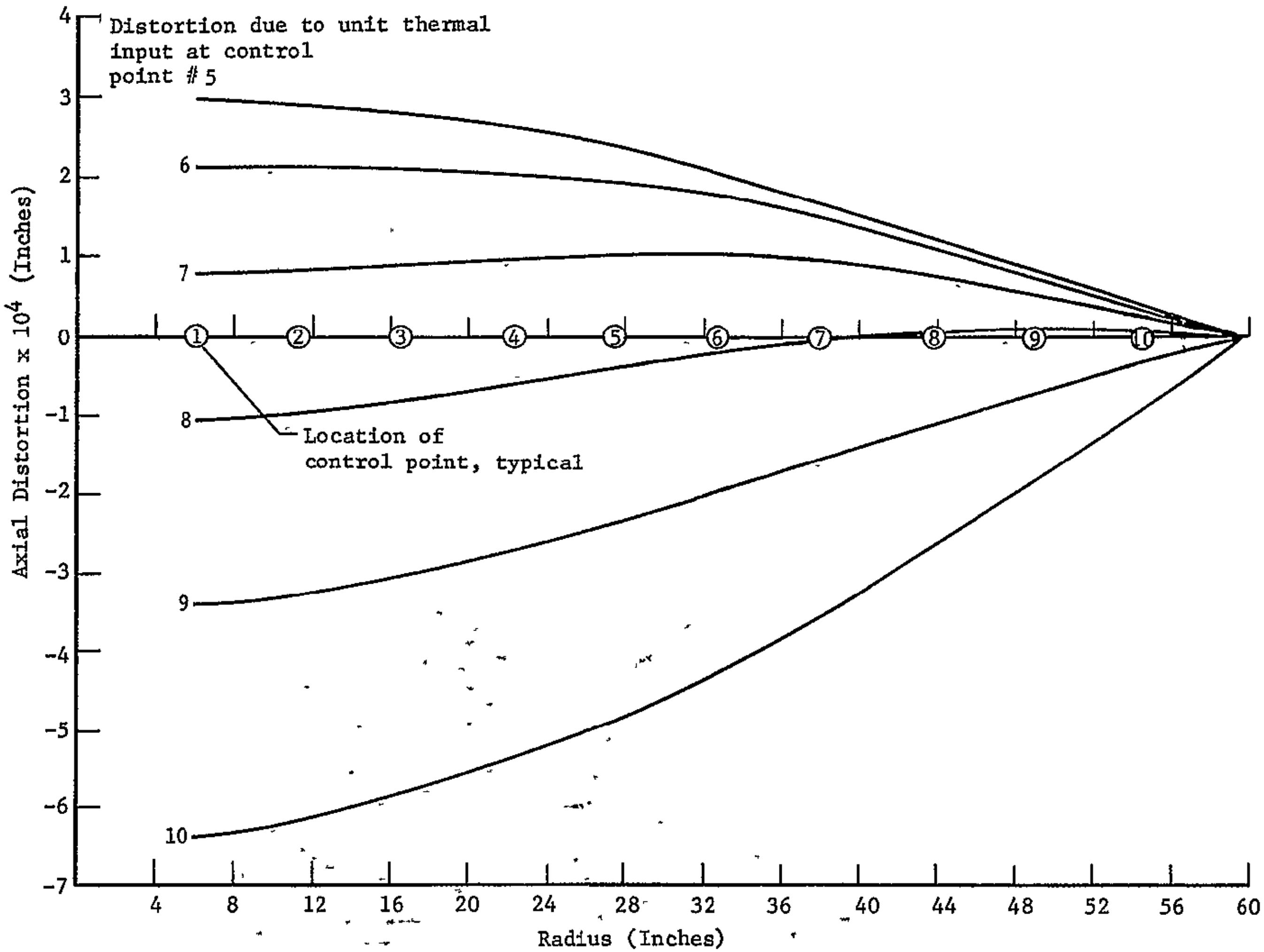

b. Thermal input applied individually at control points 5 - 10

Figure 18.- Concluded.

control points may not be an optimum selection. For a thermal active optics control system, more control points at the outer region of the mirror should be investigated. Therefore, an examination of a control system based on equal annular areas as opposed to equal meridional increments may be desirable.

The deflection influence coefficients were determined from the digital data used to plot the curves shown in Figure 18. By examining the distortion at all control points due to a unit thermal input at each control point, each column of coefficients in the flexibility matrix was determined. These coefficients are shown in Table III. This matrix was inverted using the Jordan method which has been programed for the digital computer. The Jordan method is a library subroutine known as MATINV and is available in the Langley program library. The program written to utilize this subroutine is listed in Appendix B. The stiffness matrix resulting from this inversion of the flexibility matrix is given in Table IV. These coefficients give the amplitude of the thermal input necessary to correct a given set of axial distortions at the control points. In addition to the amplitude of the thermal input, we can also determine the accuracy of the amplitude of the thermal input necessary for diffraction-limited operation. This accuracy is given by the product of the minimum contribution (minimum coefficients K_{ij}) and the maximum tolerable error. An examination of the stiffness matrix indicates that the minimum contribution is $9.19659 \times 10^{+2}$. The maximum tolerable error for diffraction-limited operation was noted previously to be 2 microinches. Therefore, the amplitude of the thermal input must

be controlled to less than

$$A = 9.19659 \times 10^{+2} \cdot 2 \times 10^{-6} \approx 1.8 \times 10^{-3}\ ^{\circ}R$$

In order to illustrate the use of the thermal active optics system, the distortions due to an acceleration-type loading were examined. The axial distortion due to a 0.01g static acceleration load was determined using the computer program of Reference 16. The axial distortion as a function of radius for this loading is shown in Figure 19. Also indicated on the figure is a sketch indicating the shell loading and positive direction of the distortion (δ). For this relatively light loading, the axial distortion exceeds the tolerance limit indicated on the figure by a factor of about 25. In order to correct this distortion, it will be necessary to introduce a distortion of equal magnitude and opposite sign by use of thermal inputs. The amplitude of the corrective thermal distortions were determined from the stiffness matrix of Table IV. These amplitudes were rounded to the nearest 0.001° R. To check the thermal inputs, the axial distortion due to both the acceleration load and the corrective thermal inputs were determined using the computer analysis of Reference 16. The combined distortion is shown in Figure 20. Also indicated on the figure is the amplitude of the thermal input for each control point. The maximum residual distortion is well within the tolerance limit of 2 microinches. It is significant that only very low amplitude inputs are necessary to correct the distortions which exceed the tolerance

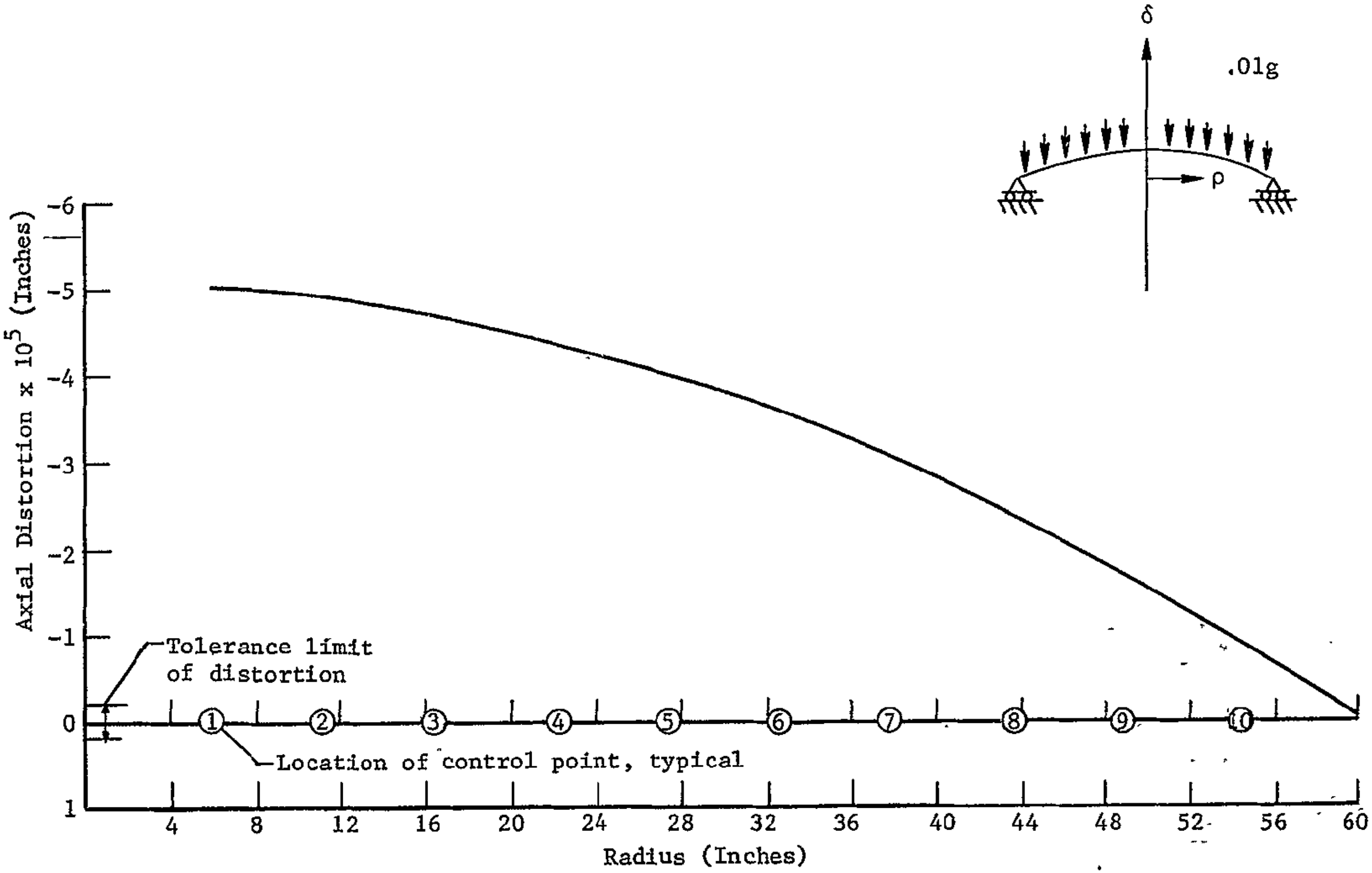

Figure 19.- Axial distortion of beryllium telescope mirror due to 0.01g acceleration type load.

Control Point	Amplitude of thermal input
1	0.152
2	0.193
3	0.166
4	0.171
5	0.166
6	0.177
7	0.155
8	0.200
9	0.103
10	0.261

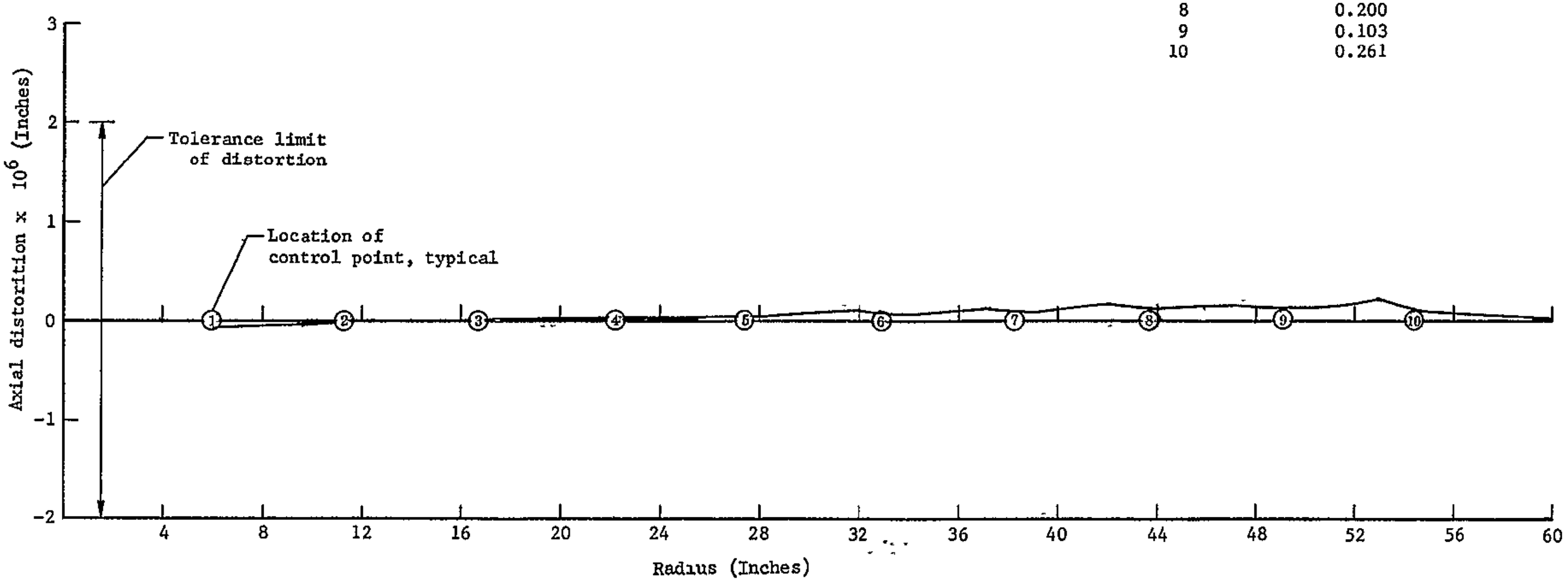

Figure 20.- Axial distortion of beryllium telescope mirror subjected to 0.01g acceleration type load and corrective thermal inputs.

limit by such a large amount. The feasibility of a thermal active optics system has thus been demonstrated for a cosine-type thermal input.

CHAPTER VI

CONCLUSIONS

A thermal active optics technique to correct distortions in a thin telescope mirror has been developed. This technique utilizes measured distortions to determine the amplitude and location of thermal inputs necessary for correction of surface errors.

The use of this technique has been demonstrated analytically by using a beryllium paraboloid. This mirror had 10 equally spaced control points actuated by symmetrical thermal inputs. The stiffness matrix indicates that for this particular configuration the amplitude of the thermal inputs must be controlled to within 1.8×10^{-3} degrees. Distortions due to an acceleration-type loading were examined. These distortions exceeded the allowable tolerance by a factor of about 25. Even though these distortions were quite large, they were corrected to well within the required accuracy. Axial temperature gradients resulting from the application of the thermal inputs to the rear surface of the mirror were shown to be quite small.

REFERENCES

1. Spitzer, Lyman, Jr.; and Boley, Bruno A.: Thermal Deformations in a Satellite Telescope Mirror. Journal of the American Optical Society, vol. 57, no. 7, July 1967, pp. 901-913.

2. Anon.: Feasibility Study of a 120-Inch Orbiting Astronomical Telescope. Prepared under NASA Contract NAS1-1305-18, American Optical Co.

3. Anon.: A System Study of a Manned Orbital Telescope. Prepared under NASA Contract NAS1-3968, NASA CR-66047, The Boeing Co., October 1965.

4. Anon.: Technology Study for a Large Orbiting Telescope. Prepared under NASA Contract NASw-1925, Itek Corporation, May 1970.

5. Robertson, Hugh J.: Development of an Active Optics Concept Using a Thin Deformable Mirror. Prepared under NASA Contract NAS1-7103, The Perkin-Elmer Corporation.

6. Livesley, R. K.: Matrix Methods of Structural Analysis. The Macmillan Company, New York, 1964.

7. Anon.: Optical Technology Apollo Extension System Phase A. Vol. III, Section III, prepared under NASA Contract NAS8-20256, Chrysler Corporation, October 1967.

8. Goggin, W. R.: Optical Materials Study Program - Final Technical Report. Prepared under DOD Contract DAAH01-69-C-0950, Perkin-Elmer Corporation, February 1970.

9. Krieth, Frank: Principles of Heat Transfer. International Textbook Company, Pennsylvania, 1961.

10. Gebhart, Benjamin: Heat Transfer. McGraw-Hill Book Co., Inc., New York, 1961.

11. Hildebrand, F. B.: Advanced Calculus for Applications. Prentiss-Hall, Inc., New Jersey, 1962.

12. Creedon, J. F.; and Robertson, H. J.: Evaluation of Multipoint Interaction in the Design of a Thin Diffraction-Limited Active Mirror. IEEE Transactions on Aerospace and Electronic Systems, vol. 5, no. 2, March 1969.

13. Sanders, J. L., Jr.: An Improved First-Approximation Theory for Thin Shells. NASA TR R-24, 1959.

14. Stern, G. S.: Thermoelastic Analysis of a Parabolic Shell. JPL Technical Report No. 32-479, NASA CR-53007, August 1963.

15. Budiansky, Bernard; and Radkowski, P. P.: Numerical Analysis of Unsymmetrical Bending of Shells of Revolution. AIAA Journal, vol. I, no. 8, August 1963.

16. Schaeffer, H. G.: Computer Program for Finite-Difference Solutions of Shells of Revolution Under Asymmetric Loads. NASA TN D-3926, May 1967.

TABLE I.- PROPERTIES OF BERYLLIUM

Property	Value
Modulus of elasticity (E)	40×10^6 psi
Poisson's ratio (ν)	0.08
Coefficient of thermal expansion (α)	6.9×10^{-6} $^{\circ}R^{-1}$
Thermal conductivity	92 Btu/ft-hr-$^{\circ}$R
Density	0.066 lb/in^3

TABLE II.- CALCULATED VALUES OF THE VIEW FACTOR AND HEAT FLUX AT EACH CONTROL POINT

Control point	Radius, ρ_m (in.)	View factor, F_{mp}	Heat flux, Q/A (Btu/hr,in^2)
1	6	0.03366	1.4229×10^{-3}
2	11.4	0.03384	1.4243×10^{-3}
3	16.8	0.03400	1.4250×10^{-3}
4	22.2	0.03413	1.4257×10^{-3}
5	27.6	0.03424	1.4264×10^{-3}
6	33.0	0.03433	1.4264×10^{-3}
7	38.4	0.03440	1.4271×10^{-3}
8	43.8	0.03444	1.4271×10^{-3}
9	49.2	0.03447	1.4278×10^{-3}
10	54.0	0.03448	1.4278×10^{-3}

TABLE III.- FLEXIBILITY MATRIX [C]

10^{-5} ×

8.751000E+00	2.711300E+01	3.264900E+01	3.343500E+01	2.956400E+01	2.105100E+01	7.761000E+00	-1.058000E+01	-3.430500E+01	-6.365200E+01
7.605000E+00	2.457600E+01	3.051900E+01	3.193600E+01	2.876700E+01	2.095500E+01	8.342000E+00	-9.335000E+00	-3.238400E+01	-6.100900E+01
6.471000E+00	2.152300E+01	2.776800E+01	2.997500E+01	2.768600E+01	2.075900E+01	9.008000E+00	-7.821000E+00	-3.000000E+01	-5.769100E+01
5.394000E+00	1.828800E+01	2.425100E+01	2.723200E+01	2.607200E+01	2.029000E+01	9.672000E+00	-6.025000E+00	-2.703000E+01	-5.345200E+01
4.404000E+00	1.513600E+01	2.043000E+01	2.360600E+01	2.361900E+01	1.929900E+01	1.014500E+01	-4.059000E+00	-2.349300E+01	-4.819800E+01
3.508000E+00	1.217900E+01	1.663100E+01	1.956900E+01	2.019500E+01	1.744600E+01	1.015900E+01	-2.115000E+00	-1.948200E+01	-4.190400E+01
2.703000E+00	9.445000E+00	1.299200E+01	1.545900E+01	1.625600E+01	1.456700E+01	9.354000E+00	-4.590000E-01	-1.516400E+01	-3.461300E+01
1.966000E+00	6.909000E+00	9.545000E+00	1.143100E+01	1.214800E+01	1.110900E+01	7.548000E+00	5.410000E-01	-1.079200E+01	-2.645600E+01
1.284000E+00	4.526000E+00	6.266000E+00	7.528000E+00	8.041000E+00	7.425000E+00	5.181000E+00	6.890000E-01	-6.744000E+00	-1.768800E+01
6.340000E-01	2.239000E+00	3.102000E+00	3.731000E+00	3.993000E+00	3.700000E+00	2.606000E+00	4.050000E-01	-3.260000E+00	-8.747000E+00

TABLE IV.- STIFFNESS MATRIX [K]

$10^5 \times$

5.928637E+00	-1.286407E+01	9.521991E+00	-3.590353E+00	1.407624E+00	-5.519662E-01	1.803175E-01	4.857122E-01	-3.711530E+00	5.930679E+00
3.364859E+00	9.707643E+00	-1.054335E+01	5.816880E+00	-2.263103E+00	8.928010E-01	-3.312262E-01	6.795628E-01	-3.942053E+00	6.189170E+00
1.551595E+00	-6.752532E+00	1.184375E+01	-1.079539E+01	5.796916E+00	-2.347737E+00	1.002699E+00	9.733403E-02	-3.582181E+00	5.947251E+00
2.975824E-01	2.352805E+00	-7.447217E+00	1.197543E+01	-1.068319E+01	5.755675E+00	-2.383516E+00	1.602814E+00	-4.273472E+00	6.211761E+00
7.504477E-02	-5.363172E-01	2.641169E+00	-7.592084E+00	1.193068E+01	-1.058672E+01	5.748426E+00	-1.897596E+00	-2.667380E+00	5.531911E+00
2.350126E-02	2.067805E-02	-4.446770E-01	2.549068E+00	-7.548588E+00	1.184366E+01	-1.046296E+01	6.241817E+00	-6.247341E+00	7.053590E+00
2.380006E-02	-7.008097E-02	1.098127E-01	-4.253789E-01	2.487638E+00	-7.523182E+00	1.181751E+01	-9.894527E+00	1.977602E+00	3.688732E+00
2.969810E-02	-5.511088E-02	1.663136E-02	6.352284E-02	-3.959441E-01	2.418422E+00	-7.419858E+00	1.226071E+01	-1.424228E+01	1.134455E+01
1.104724E-02	-2.855116E-02	3.283121E-02	-3.255498E-02	4.557908E-02	-3.284748E-01	2.328327E+00	-6.824432E+00	8.022138E+00	-3.371034E+00
4.027101E-02	-8.749585E-02	5.383443E-02	9.196590E-03	-1.924112E-02	-1.892907E-02	-2.250223E-01	2.864666E+00	-1.129168E+01	1.504815E+01

APPENDIX A

DIGITAL COMPUTER PROGRAM TO GENERATE THE STEADY-STATE TEMPERATURE DISTRIBUTION IN A CIRCULAR DISC

```
JOB.                    A0301,      1,MARVIN RHODES    ,RD0212,1148,2011
RUN(S)
SETINDF.
LGO.
      PROGRAM  MDR          (INPUT,OUTPUT,TAPE5=INPUT,TAPE6=OUTPUT)
C THIS PROGRAM WILL GENERATE THE STEADY STATE TEMPERATURE DISTRIBUTION
C IN A DISC OF THICKNESS T
      EXTERNAL FUNC
      COMMON XLAM(20),I
      DIMENSION D(1),FOFX(1),ANSJN(400),ANSJ(400),ANS(400),F(20)
C GENERATES B(N) COEFFICIENTS DESIGNATED AS F(N)
      PRINT 3
    3 FORMAT ( * COEFF. NUMBER    LAMBDA        BESSELS FUNCTION    COEF
     1F. VALUE*)
      READ 1, A,B,N
    1 FORMAT (2F10.5,I6)
      DO 7 I=1,20
   10 READ 2,XLAM(I)
    2 FORMAT (E16.8)
      CALL MGAUSS(A,B,N,D,FUNC,FOFX,1)
      CALL BSSLS(XLAM(I),ANSJN,0,IERR)
      C=ANSJN(1)*ANSJN(1)
      E=1.0+EXP(-XLAM(I)/25.)
      F(I)=-2.*D(1)/(C*E)
      PRINT 4,I,XLAM(I),ANSJN(1),F(I)
    4 FORMAT ( 5X,I3,3X,E16.8,3X,E16.8,3X,E16.8)
    7 CONTINUE
C GENERATES TEMPERATURE AT 0.05 RADIAL INCREMENTS FOR EACH VALUE OF ZETA
   30 IF(EOF,5)70,20
   20 READ 15,Z
   15 FORMAT(F10.5)
      PRINT 17,Z
   17 FORMAT(3H Z=,F10.5,2HXL)
      PRINT 18
   18 FORMAT(6X,6HRADIUS,12X,11HTEMPERATURE,/)
      R=0.0
   40 T=1.0
      DO 50 I=1,20
      G=XLAM(I)*R
      CALL BSSLS(G,ANS,0,IER)
```

```
      H=EXP(XLAM(I)*(Z-2.)/50.)+EXP(-XLAM(I)*Z/50.0)
      HH=F(I)*ANS(1)*H
      T=T+HH
   50 CONTINUE
      PRINT 60,R,T
   60 FORMAT(E16.8,5X,E16.8)
      R=R+0.05
      IF(R.LT.1.05) GO TO 40
      GO TO 30
   70 STOP
      END
      SUBROUTINE FUNC(R,FOFX)
      DIMENSION FOFX(1),ANSJ(400)
      COMMON XLAM(20),I
      A=COS(6.283185307*R)
      B=XLAM(I)*R
      CALL BSSLS(B,ANSJ,0,IERR)
      FOFX(1)=R*A*ANSJ(1)
      RETURN
      END
```

APPENDIX B

DIGITAL COMPUTER PROGRAM TO INVERT THE FLEXIBILITY MATRIX C

TO OBTAIN THE STIFFNESS MATRIX K

```
JOB,1,0400, 45000.          A0301,       1, MARVIN RHODES , RD0212, 1148,2011
RUN(S)
SETINDF.
LGO.
NOMAP.
      PROGRAM MAT   (INPUT,OUTPUT,TAPE5=INPUT,TAPE6=OUTPUT)
C THIS PROGRAM WILL INVERT A MATRIX CALLED A BY SUBROUTINE MATINV. INPUT DATA
C IS NR(NUMBER OF ROWS) FOLLOWED BY MATRIX A DATA READ BY ROWS. INPUT AND
C OUTPUT FORMAT STATEMENTS (2 AND 4 ) MUST BE CHANGED FOR EACH MATRIX.
      DIMENSION A(100,100),B(100,1),IPIVOT(100),INDEX(100,2)
      DIMENSION DELTA(10),T(10)
      READ 1,NR
    1 FORMAT (I3)
      READ 2,((A(I,J),J=1,NR),I=1,NR)
    2 FORMAT((10F8.5))
      PRINT 3
    3 FORMAT (//40X,*ORIGINAL MATRIX*///)
      PRINT 4,((A(I,J),J=1,NR),I=1,NR)
      CALL MATINV(A,NR,B,0,DETERM,IPIVOT,INDEX,100,ISCALE)
      PRINT 5
    5 FORMAT(//40X,*INVERSE OF MATRIX A*///)
      PRINT 4,((A(I,J),J=1,NR),I=1,NR)
    4 FORMAT((10E13.6,//))
      DET=10.**(100*ISCALE)*DETERM
      PRINT 6, DET
    6 FORMAT (///*VALUE OF DETERMINATE IS *E16.8)
      READ 7,(DELTA(I),I=1,10)
    7 FORMAT(10F8.6)
      DO 9 I=1,10
      T(I)=0.0
      DO 8 J=1,10
    8 T(I)=A(I,J)*DELTA(J)+T(I)
      PRINT10,I,T(I)
   10 FORMAT(* TEMP*,I2,*=*,E16.8)
    9 CONTINUE
      STOP
      END
```